https://doi.org/10.5194/acp-2022-422
Preprint. Discussion started: 5 July 2022

Atmospheric Chemistry and Physics Discussions

Impacts of reductions in non-methane short-lived climate forcers on future climate extremes and the resulting population exposure risks in Asia

Yingfang Li[1], Zhili Wang[1,2*], Yadong Lei[1], Huizheng Che[1], Xiaoye Zhang[1]

[1]State Key Laboratory of Severe Weather and Key Laboratory of Atmospheric Chemistry of CMA, Chinese Academy of Meteorological Sciences, Beijing, 100081, China

[2]Collaborative Innovation Center on Forecast and Evaluation of Meteorological Disasters (CIC-FEMD), Nanjing University of Information Science & Technology, Nanjing, 210044, China

Correspondence to: Zhili Wang (wangzl@cma.gov.cn)

Abstract. Non-methane short-lived climate forcers (SLCFs), including aerosols, ozone, and their precursors, are important climate forcings and primary air pollutants. Stringent SLCF emissions controls to mitigate air pollution have been implemented by various governments, which will substantially impact the future climate. We investigate the changes in future climate extremes and resulting population exposure risks in Asia during 2031–2050 in response to non-methane SLCF emissions reductions using multi-model ensemble (MME) simulations under two scenarios (SSP3-7.0 and SSP3-7.0-lowNTCF) with different air quality control measures from the Aerosol and Chemistry Model Intercomparison Project (AerChemMIP), which is endorsed by Coupled Model Intercomparison Project phase 6 (CMIP6). The MME results show that future reductions in non-methane SLCF emissions lead to an increase of 0.23 W m^{-2} in global annual mean effective radiative forcing, thereby magnifying the greenhouse gas (GHG)-induced global surface warming by 0.19 K during 2031–2050. The additional warming caused by the non-methane SLCF reductions increases the regional average temperature on the hottest days (TXx) by 0.3 K, the percentage of warm days (TX90p) by 4.8%, the number of tropical nights (TR) by 1.7 days, the warm spell duration (WSDI) by 1.0 days, the number of heavy precipitation days (R10) by 1.3 days, the maximum consecutive 5-day precipitation (RX5day) by 0.8 mm, and the total wet-day precipitation (R95p) by 16.4 mm during 2031–2050. For temperature extremes, the largest regional increases of TXx, TX90p, and WSDI occur in northern India (NIN) and northern China (NC). Relatively large increases in TR are predicted in NC and the Sichuan Basin (SCB), reaching 5.1 days and 4.9 days, respectively. For precipitation extremes, the regional changes are greatest in southern China (SC), particularly southwestern China (SWC), where reductions of non-methane SLCF emissions increases R10 by 3.0 days, RX5day by 2.2 mm, and R95p by 39.5 mm. Moreover, the populations exposed to temperature and precipitation extremes increase most sharply in NIN, reaching (32.2 ± 11.4) × 10^7 person-days and (6.7 ± 7.8) × 10^6 person-days during 2031–2050, respectively, followed by NC and SCB. Our results highlight the significant impacts of non-methane SLCF reductions on future climate extremes and related exposure risks in Asia, which are comparable to the impact associated with increased GHG forcing in some regions.

https://doi.org/10.5194/acp-2022-422
Preprint. Discussion started: 5 July 2022

Atmospheric Chemistry and Physics Discussions

1 Introduction

Short-lived climate forcers (SLCFs), also known as near-term climate forcers (NTCFs), include aerosols (e.g., sulfates, black carbon (BC), organic carbon (OC), ammonium salts, and nitrate), ozone, methane (CH_4), and their precursors (e.g., sulfur dioxide (SO_2), nitrogen oxides (NOx), carbon monoxide (CO), and ammonia) (Myhre et al., 2013). Since the beginning of the industrial era, human activities have led to a significant increase in emissions of SLCFs (Hoesly et al., 2018). Non-methane SLCFs, including aerosols, ozone, and their precursors, affect not only climate but also air quality. Previous studies have revealed significant influences of non-methane SLCFs on global and regional climate as well as human health (Liao et al., 2015; Forster et al., 2021; Apte et al., 2015; Malley et al., 2017; Xie et al., 2016a).

According to the Sixth Assessment Report of the Intergovernmental Panel on Climate Change (IPCC, AR6), global average effective radiative forcing (ERF) since the beginning of the industrial revolution (1750–2019) is –1.1 (–1.7 to –0.4) W m^{-2} for aerosols and +0.47 (+0.24 to +0.71) W m^{-2} for ozone (Forster et al., 2021). Over the past few decades, climate change caused by non-methane SLCFs has had an important impact on natural ecosystems and human societies in Asia (Ramanathan et al., 2007; Li et al., 2016). Surface cooling and tropospheric atmospheric thermal responses associated with aerosol forcing can weaken the East Asian summer monsoon, thereby suppressing precipitation in the East Asian monsoon region (Li et al., 2016; Xie et al., 2016b; Wang et al., 2019, 2020; Mu and Wang, 2021). The increase in aerosols since the 1950s may have led to weakening of summer precipitation in South Asia (Bollasina et al., 2011) and the anomalous precipitation pattern described as “southern flood/northern drought” in eastern China (Li et al., 2016). Regional aerosol-cloud interactions may be the main factor causing extreme precipitation variability in India and China during 1979–2005 (Lin et al., 2018). In terms of ozone, Chang et al. (2009) noted that tropospheric ozone increased average surface air temperature (SAT) by 0.43°C and decreased average precipitation by 0.08 mm day^{-1} in eastern China during 1971–2000. The simulation results of Li et al. (2018) showed that East Asian summer monsoon circulation was enhanced over southern China but weakened over northern China during 2001–2010 due to tropospheric ozone forcing.

Emissions controls implemented by governments, which aim to mitigate global warming and improve air quality, have led to significant changes in non-methane SLCF emissions that will affect future climate change (Naik et a., 2021). Meanwhile, the important role of non-methane SLCFs in historical climate change in Asia (Bollasina et al., 2011; Dong et al., 2019; Wang et al., 2019) suggests that SLCF emissions reductions may have major implications for future regional climate and its extremes (Wang et al., 2016; Zhang et al., 2018; Wilcox et al., 2020). In previous research, the assessed impact of reducing non-methane SLCF emissions on future climate change has been limited to the effect of aerosol forcing associated with incomplete interactive tropospheric chemistry schemes in global climate models. Future aerosol emissions reductions could greatly aggravate the warming effect caused by greenhouse gas (GHG) forcing (Lin et al., 2016; Hienola et al., 2018), particularly in eastern and southern Asia, and may increase surface temperatures by 0.5°C in some regions (Westervelt et al., 2015; Chuwah et al., 2016) and cause a significant increase in extreme high-temperature events (Wang et al., 2016; Samset et al., 2018; Luo et al., 2020). Future aerosol reductions may also shift the tropical rain belt northwards, enhancing precipitation in the Asian

https://doi.org/10.5194/acp-2022-422
Preprint. Discussion started: 5 July 2022


Atmospheric Chemistry and Physics Discussions

monsoon region (Westervelt et al., 2018; Zanis et al., 2020) and shifting both the mean and extreme values of precipitation toward larger values (Zhao et al., 2018). Asia is a region where extreme precipitation is particularly sensitive to aerosol reductions (Lin et al., 2016; Samset et al., 2018).

The precursors of aerosols and ozone are homologous and overlapping (e.g., NOx, volatile organic compounds (VOCs)) (Myhre et al., 2013). Implementation of air pollution control measures inevitably causes simultaneous changes in their radiative forcings. Therefore, considering the impacts of changes in non-methane SLCFs on future climate, particularly on regional extreme climate events, is essential. However, few studies in this field have been conducted to date. A recent study considering emissions reductions of aerosols, ozone, and their precursors showed that future non-methane SLCF reductions will not only improve air quality but also increase global mean temperature, precipitation, and climate extremes in the mid-21st century, with more marked warming and wetting trends in some regions, particularly Asia and the Arctic (Allen et al., 2020). However, that study focused on trends of climate variables, and its assessment of regional climate changes, particularly climate extremes, was insufficient. Although the IPCC AR6 assesses the climate effects of future changes in non-methane SLCFs, it focuses on global averages, with little regional assessment, particularly in Asia where non-methane SLCF emissions are extremely high (Naik et al., 2021).

With the continued global warming caused by GHG emissions, the frequency of climate extremes increases (Zhou and Qian, 2019), increasing the threat to human health, economic stability, and environmental sustainability. As a densely populated and climate-vulnerable region, Asia is at high risk for future population exposure to climate extremes. In the coming decades, the population exposed to extreme heat in East Asia will continue to increase under most future scenarios (An et al., 2020). The population exposure to extreme precipitation over the Indus River Basin is projected to increase by 72.4%, 122.7%, and 87.6%, respectively, with global warming of 1.5°C, 2.0°C, and 3.0°C (Zhao et al., 2021). The population affected by extreme precipitation in China is projected to increase by nearly 22% by the end of the 21st century under the representative concentration pathway–shared socioeconomic pathway (RCP-SSP) scenario RCP4.5-SSP2, with the largest absolute increase in eastern China (Chen and Sun, 2020). With increasing warming in the future, dry conditions across China will be further aggravated, and an additional 12.9 million people will be exposed to droughts under the 1.5°C global warming scenario (Chen et al., 2018; Chen and Sun, 2019). This raises the issue of whether reductions in non-methane SLCF emissions will further exacerbate the intensity and frequency of extreme climate events and the resulting risk of population exposure.

With continuous development, some climate system models have become more complete Earth system models (ESMs), which consider the coupling of Earth system processes and support relatively realistic and complete analysis of the whole Earth-atmosphere system. Furthermore, the Aerosols and Chemistry Intercomparison Project (AerChemMIP) was established by the CMIP6 to comprehensively assess the impacts of SLCFs on climate and air quality (Collins et al., 2017), which can further elucidate changes in atmospheric chemical composition and their interactions with changes in global and regional climate. Here, we quantify the impacts of non-methane SLCF emissions reductions on extreme climate changes and the resulting population exposure risks during 2031–2050 in Asia using historical simulations and two scenario simulations (SSP3-7.0 and SSP3-7.0-lowNTCF) with state-of-the-art ESMs from the AerChemMIP (Collins et al., 2017).

https://doi.org/10.5194/acp-2022-422
Preprint. Discussion started: 5 July 2022


Atmospheric Chemistry and Physics Discussions

The remainder of this paper is organized as follows. Section 2 describes the models, simulations, and calculations of climate extremes and related population exposure. Section 3 contains the results. Finally, our discussion and conclusions are presented in Section 4.

2 Methods

2.1 Future emissions scenarios

Simulations under two AerChemMIP scenarios, SSP3-7.0 and SSP3-7.0-lowNTCF, were performed to assess the impacts of non-methane SLCF changes on climate and air quality (Collins et al., 2017; Allen et al., 2020). The SSP3-7.0 scenario is used as the reference scenario (~7.0 W m^{-2} at 2100), as it includes no climate policies related to GHG reductions and weak air pollution controls. In this scenario, the future climate change is approximatively influenced by GHG forcing only. The perturbation scenario SSP3-7.0-lowNTCF uses the same GHG forcing path but with strong air pollution controls, and thus future climate change in this scenario is influenced by a combination of GHG forcing and reduction of non-methane SLCF emissions. As shown in Figure 1, the two simulations include the same variation in carbon dioxide (CO_2) and CH_4, both of which continue to increase in the future. However, non-methane SLCFs exhibit different changes in these two scenarios. Global emissions of non-methane SLCFs are maintained at a stable level or vary slightly after 2020 under the SSP3-7.0 scenario, with a decrease of 1% in SO_2 and increases of 7–13% in other SLFCs by 2050. Global emissions of all non-methane SLCFs show significant downward trends under the SSP3-7.0-lowNTCF scenario, ranging from 10% for BC to 55% for SO_2 by 2050. Assuming that the joint impact of GHGs and non-methane SLCFs are approximated as a linear superposition of their respective impacts, the impact of non-methane SLCF mitigation can be quantified as the difference between the results of simulation under the two scenarios (SSP3-7.0-lowNTCF minus SSP3-7.0) (Allen et al., 2020).

2.2 Models and simulations

Seven CMIP6 ESMs with interactive representation of tropospheric aerosols and atmospheric chemistry were used to conduct the SSP3-7.0 and SSP3-7.0-lowNTCF simulations (Table 1), with integration periods of 2015–2055 and individual models integrated through 2100. We used the daily and monthly outputs for both scenarios from 2015 to 2050. Historical climate simulations (Historical) for 1995–2014 from the same models were used as the reference period. In addition to coupled ocean-atmosphere simulations, these models were also used for Atmospheric Model Intercomparison Project (AMIP)-style simulations with the time-varying sea surface temperature (SST) outputs from SSP3-7.0 simulations under the two emissions scenarios to quantify the ERF associated with future changes in atmospheric composition (Collins et al., 2017). ERF is a measure of the extent to which forcing agents affect climate, defined as the change in net radiative flux at the top of the atmosphere caused by a disturbance that allows for changes in atmospheric temperature, water vapor, and clouds, but keeps global SST unchanged (Myhre et al., 2013; Forster et al., 2016; Pincus et al., 2016). All model outputs were interpolated into a 1° × 1° grid through bilinear interpolation.

https://doi.org/10.5194/acp-2022-422
Preprint. Discussion started: 5 July 2022


Atmospheric Chemistry and Physics Discussions

2.3 Climate extremes indices

Following the definitions of the Expert Team for Climate Change Detection and Indices, six extreme temperature indices and four extreme precipitation indices representing intensity and frequency were employed in this study (Table 2). Due to incomplete data provided by CESM2-WACCM and GISS-E2-1-G, the extreme temperature indices were calculated with the remaining five models, and the extreme precipitation indices were calculated with the six models other than GISS-E2-1-G. We focused on the changes in extreme climate indices in the future (2031–2050) relative to the reference period (1995–2014).

2.4 Population exposure

Population exposure to climate extremes can be estimated by multiplying the frequency of extreme events by the number of people, and this method has been widely employed to assess future climate risks (Jones et al., 2015). Gridded population datasets for 2000 and 2040 under SSP3 were used to represent the population during the reference and future periods, respectively. These population datasets were summed for each grid box of 1° × 1° to match the resolution of the climate data. Population exposures to extreme heat and heavy precipitation were are calculated as the population exposed multiplied by the number of days with a daily maximum temperature greater than the 90th percentile of the reference period and by the number of days with daily precipitation greater than the 95th percentile of the reference period, respectively (Chen et al., 2020; Sun et al., 2022). The exposure change (Δexpo) could be decomposed into three parts, namely, changes driven by the climate effect, the population effect, and their interaction:

$$\Delta expo = (c + \Delta c) \cdot (p + \Delta p) - c \cdot p = c \cdot \Delta p + p \cdot \Delta c + \Delta c \cdot \Delta p \,, \quad (1)$$

where c and p are the number of extreme days and population in the baseline period, respectively. Δc and Δp are the changes in climate extreme days and population in the future with respect to the baseline period. Thus, the terms of c·Δp, p·Δc, and Δc·Δp represent the population, climate, and interaction effects, respectively, on exposure changes, allowing for attribution analysis of changes in population exposure.

3 Results

3.1 Changes in global ERF and SAT

Figure 2 shows the spatial patterns of ERF under the SSP3-7.0 and SSP3-7.0-lowNTCF scenarios and their changes associated with reductions in non-methane SLCF emissions during 2031–2050 relative to 1995–2014. As GHG concentrations increase and SLCF concentrations decrease, more long-wave radiation is absorbed and less short-wave radiation is reflected, resulting in positive global average ERF values under both scenarios (Fig. 2a and b). Non-methane SLCF emissions reductions lead to positive ERF over most of the globe, particularly in the Northern Hemisphere (Fig. 2c). Increases in ERF of approximately 1 W m^{-2} occur mainly in Eurasia north of 40°N, the northern Pacific Ocean, northern America, and the northern Atlantic Ocean. The largest increases of more than 1.5 W m^{-2} are found over India, southeastern Asia, and surrounding oceans

https://doi.org/10.5194/acp-2022-422
Preprint. Discussion started: 5 July 2022


Atmospheric Chemistry and Physics Discussions

(Fig. 2c). Notably, some negative ERFs remain over northern China, the Sichuan Basin, Arabian Peninsula, and northern Africa, as the increase in low cloud cover induced by changes in regional precursor concentrations leads to greater reflection of shortwave radiation (Yang et al., 2017; Zhang et al., 2018). The multi-model ensemble (MME) global annual mean ERF induced by non-methane SLCF emissions reductions is +0.23 W m^{-2}, with positive values obtained from all models except GFDL-ESM4 (Table 3).

Figure 3 shows the MME global changes in SAT under each scenario. Increases in SATs occur worldwide during 2031–2050 under both the SSP3-7.0 and SSP3-7.0-lowNTCF scenarios (Fig. 3a and b). The SAT increases are greater in the Northern Hemisphere and on land than in the Southern Hemisphere and ocean areas due to greater precursor emissions in the Northern Hemisphere and the high heat capacity of the ocean. Regionally, the greatest warming of more than 1.5 K is found in central and northern Asia and in northern North America, particularly in the Arctic, where warming is greater than 2.5 K. Moreover, such warming is exacerbated by future non-methane SLCF emissions reductions in most regions of the world, particularly in the Northern Hemisphere (Fig. 3c). Previous studies have shown that reduction of sulfate aerosols is the dominant driver of future SAT increases in response to aerosol forcing, particularly in the Northern Hemisphere (Baker et al., 2015; Samset et al., 2018). Future reductions in non-methane SLCF emissions causes additional warming of more than 0.2 K throughout Eurasia, the northern Pacific, and northern North America. In particular, warming in the Arctic will exceed 0.6 K (Fig. 3c). The reduction of non-methane SLCF emissions results in an average increase of 0.19 K in global mean SAT in the MME results, ranging from 0.06 K to 0.29 K across different models (Table 3). Furthermore, the increase in global mean SAT is consistent with the increase in global mean ERF except for GFDL-ESM4. However, warming and positive ERF do not correspond exactly in some regions, such as the Arctic and northern China (Figs. 2c and 3c), likely due to climate feedbacks, remote teleconnection, and other processes. In general, the combined reductions of aerosols, ozone, and their precursors causes further warming, suggesting that the cooling effect of ozone reduction is significantly weaker than the warming effect of aerosol reduction.

3.2 Changes in temperature extremes in Asia

Figure 4 shows the time series of changes in annual mean extreme temperature indices averaged across Asia under the SSP3-7.0 and SSP3-7.0-lowNTCF scenarios from 2015 to 2050 relative to the reference period. All extreme temperature indices in Asia consistently increase under both scenarios, with a larger increase under the SSP3-7.0-lowNTCF scenario. By 2050, TXx and TX90pincrease by 2.2 K and 27.7% under the SSP3-7.0 scenario and by 2.6 K and 34.9% under the SSP3-7.0-lowNTCF scenario, respectively. Compared to TXx and TX90, larger increases occur in TNn and TN90p, which increase by 2.8 K and 35.9% under the SSP3-7.0 scenario and 3.2 K and 43.1% under the SSP3-7.0-lowNTCF scenario, respectively. These changes indicate that future nighttime warming will be more apparent than daytime warming under both scenarios. Compared to the SSP3-7.0 scenario, non-methane SLCF emissions reductions cause additional warming of about 0.43 K for both TXx and TNn and increases of about 7.1% for both TX90p and TN90p. In addition, non-methane SLCF emissions reductions increases the TR and WSDI by 2.8 and 2.2 days by 2050, respectively.

https://doi.org/10.5194/acp-2022-422
Preprint. Discussion started: 5 July 2022


Atmospheric Chemistry and Physics Discussions

Figure 5 shows the spatial patterns of changes in TXx, TX90p, TR, and WSDI over Asia during 2031–2050 relative to the reference period. Consistent increases occur in these extreme temperature indices under both the SSP3-7.0 and SSP3-7.0-lowNTCF scenarios. For TXx, the warming is greater at higher latitudes under both scenarios, but the magnitude of the increase is larger under the SSP3-7.0-lowNTCF scenario than the SSP3-7.0 scenario. Compared to the reference scenario, non-methane SLCF reduction leads to an additional increase of about 0.2 K across most of the Asian continent. Local effects of non-methane SLCF reductions are particularly large due to the short lifetimes of these contaminants. For example, future reductions in non-methane SLCFs cause TXx increases of more than 0.4 K in northern India and northern China, where anthropogenic emissions are high (Fig. 5c).

Similarly, TX90p increases under both scenarios (Figs. 5d and e). In contrast to the changes in SAT (Fig. 2) and TXx, the increase in TX90p is more pronounced (>40%) at lower latitudes. This difference arises because high temperatures and lower daily temperature variation at low latitudes result in more days above the 90th percentile of the reference period. The largest increases in TX90p with non-methane SLCF reductions are found over India and eastern China, where increases are more than 8% and around 6%, respectively (Fig. 5f). In these regions, the effects of non-methane SLCFs are comparable to those of GHG forcing (Fig. 5d and f). TXx and TX90p indicate an increase in extreme daytime heat events, which not only increases the risk for heatstroke but also exacerbates ozone pollution, posing a further threat to human health (Gosling et al., 2009; Pu et al., 2017).

Concomitant with the increases in TNn and TN90p, TR is also predicted to increase over Asia in the future. A significant increase of more than 40 days occurs in parts of southern India, the Indo-China Peninsula, and Indonesia, followed by eastern and northern China and Mongolia, with increases greater than 30 days, under the SSP3-7.0 scenario (Fig. 5g). The spatial pattern of TR changes under SSP3-7.0-lowNTCF is similar to that under SSP3-7.0, but the magnitude of the changes is larger (Fig. 5g and h). Non-methane SLCF reductions cause the largest increases in TR of more than 5 days in the Indo-China Peninsula, northern and northeastern China, and the Korean Peninsula (Fig. 5i). Notably, TR indicates that the temperature at night remains above 20°C. High nighttime temperatures can cause insomnia and abnormalities in thermoregulation, which may increase health risks, particularly for elderly or sick individuals (Fischer and Schär, 2010; Gosling et al., 2009).

With the increase in average temperature and values of extreme temperature indices described above, WSDI is also predicted to increase significantly across Asia under both scenarios (Fig. 5j and k). Similar to TX90p, the increase in WSDI is more apparent at lower latitudes. The largest increments occur over the Qinghai-Tibet Plateau, southern China, and the Indo-China Peninsula. Compared to the SSP3-7.0 scenario, the increase in WSDI is greater under the SSP3-7.0-lowNTCF scenario, with increases of more than 12 days in the Qinghai-Tibetan Plateau, the Indo-China Peninsula, and along the coast of southern China. Non-methane SLCF reductions are associated with increases in WSDI of more than 2 days over almost the entire Asian continent and more than 4 days in parts of northern China, coastal areas of southern China, northern India, and central and northern Asia (Fig. 5l).

Overall, the combined reductions of aerosols, ozone, and their precursors have an additional warming effect on Earth's climate system, exacerbating the surface warming and extreme temperature events caused by GHGs. These results are

https://doi.org/10.5194/acp-2022-422
Preprint. Discussion started: 5 July 2022


Atmospheric Chemistry and Physics Discussions

consistent with studies considering only aerosol reductions (Wang et al., 2016; Samset et al., 2018). Spatially, non-methane SLCF reductions cause the largest increases in extreme temperature indices in northern India and eastern China. In these regions, the human and environmental effects of temperature extremes are more significant due to high population densities and industrial development. Therefore, we selected northern India (NIN), northern China (NC), southern China (SC), and the Sichuan Basin (SCB) (Fig. 6a) for quantitative assessment of changes in regional mean extreme temperature indices in response to non-methane SLCF reductions.

The domain-averaged values of TXx, TX90p, TR, and WSDI across Asia have increases of 1.4 K, 37.4%, 8.9 days, and 9.1 days under the SSP3-7.0 scenario, respectively (Fig. 6). Considering the effects of non-methane SLCF reductions, these extreme temperature indices show increases of 1.7 K, 42.2%, 10.6 days, and 10.1 days under the SSP3-7.0-lowNTCF scenario, respectively. In general, the SCB is most strongly affected by extreme temperatures under both scenarios. Future reductions in non-methane SLCFs result in additional increases of 0.3 K in TXx, 4.8% in TX90p, 1.7 days in TR, and 1.0 days in WSDI for Asia. TXx, TX90p, and WSDI all show their largest regional increases in northern India and northern China, reaching 0.5 K, 8.5%, and 2.8 days and 0.4 K, 5.9%, and 3.0 days, respectively. The models agree on the sign of the change in TR across regions, and the largest increases occur in NC and the SCB, at 5.1 and 4.9 days, respectively. Although the MME changes in regional mean extreme temperature indices are consistently positive, some differences are found among the models, which may be attributed to differences in model resolution, the types of SLCFs included in each model, and parameterization schemes (Allen et al., 2020; Wei et al., 2019).

3.3 Changes in precipitation extremes in Asia

Figure 7 shows the time series of changes in annual mean precipitation indices averaged across Asia under the SSP3-7.0 and SSP3-7.0-lowNTCF scenarios from 2015 to 2050 relative to the reference period. Similar to the extreme temperature changes described above, the extreme precipitation changes are more significant under the SSP3-7.0-lowNTCF scenario than the SSP3-7.0 scenario, and this difference increases gradually after 2030. By 2050, the values of R10, RX5day, and R95p have increased by 1.7 days, 2.0 days, and 42.0 mm under the SSP3-7.0 scenario, respectively. The increases in precipitation decrease drought events, resulting in a reduction in maximum CDD of 2.4 days. The non-methane SLCF reductions increase both R10 and RX5day by 1 day and R95p by 15.3 mm, but reduce CDD by 1 day (green dashed lines in Fig. 7).

Figure 8 shows the spatial patterns of extreme precipitation indices over Asia. Considering the spatial distribution of the changes in extreme precipitation indices, we selected NIN, NC, SC, and southwestern China (SWC) (Fig. 9a) for quantitative analysis of extreme precipitation changes. R10, RX5day, and R95p represent future changes in the intensity and frequency of extreme heavy precipitation. Under the SSP3-7.0 scenario, R10 decreases by approximately 2 days in central Asia, central India, the southeastern Qinghai-Tibet Plateau, SWC, and the Indo-China Peninsula, and by more than 4 days in parts of Indonesia, while it increases in all other regions of Asia (Fig. 8a). Under the SSP3-7.0-lowNTCF scenario, R10 increases by 2.1 days across Asia, with the most significant increases of 3.8 days in SC and near the Himalayas. The reductions in non-methane SLCFs cause an increase of 1.3 days in average R10 across Asia. For the selected regions, the largest increases in

https://doi.org/10.5194/acp-2022-422
Preprint. Discussion started: 5 July 2022


Atmospheric Chemistry and Physics Discussions

R10 occur in SWC and SC, reaching 3.0 days and 2.2 days, respectively (Fig. 9b). In addition, significant increases of more than 3.0 days in R10 in are found in the southeastern Qinghai-Tibet Plateau, India, the Indo-China Peninsula, and Indonesia; this pattern is exactly opposite of that of GHG forcing (Fig. 8a and c). By contrast, previous research suggested that reduction of aerosols alone will reduce R10 in these regions during 2031–2050 (Wang et al., 2016; Zhao et al., 2018).

RX5day increases across most of Asia under both future scenarios (Fig. 8d and e), with average increases of 1.4 mm and 2.2 mm under the SSP3-7.0 and SSP3-7.0-lowNTCF scenarios, respectively. The largest increases among the selected regions occur in SC, at 2.1 mm and 3.4 mm, respectively (Fig. 9c). Future reductions in non-methane SLCFs leads to an increase of 0.8 mm in RX5day in Asia. Regionally, these effects of non-methane SLCF reductions are much greater than the effects of GHG forcings alone. For example, non-methane SLCF mitigation yields an increase of 2.2 mm in RX5day in SWC, compared to 0.2 mm under the SSP3-7.0 scenario (Fig. 9c). In addition, non-methane SLCF reductions cause a significant increase of more than 2 mm in RX5day in the southeastern Qinghai-Tibet Plateau, the western Hengduan Mountains, and the middle and lower reaches of the Yangtze River, whereas decreases of more than 3 mm occur in the southwestern part of the Indo-China Peninsula (Fig. 8f). The variation in RX5day can be used as an indicator of flooding and related hazards (Frich et al., 2002; Sillmann et al., 2013). Our results suggest that heavy precipitation associated with natural disasters will be aggravated in some parts of Asia in the future due to non-methane SLCF reductions.

The spatial pattern of changes in R95p is consistent with that of RX5day. With or without strong air quality controls, R95p increases across most of Asia, reaching 35.4 mm and 51.8 mm, respectively (Fig. 8g and h). The increases in R95p exceed 120 mm in the Himalayas, southeastern Qinghai-Tibet Plateau, western Hengduan Mountains, and Indonesia under the SSP3-7.0-lowNTCF scenario (Fig. 8h). Additional increases in R95p caused by reduced emissions of non-methane SLCFs are apparent in the western Hengduan Mountains (>60 mm), while significant decreases occur in the southwestern part of the Indo-China Peninsula (<-50 mm). R95p also decreases (<-10 mm) along the coast of SC (Fig. 8i), with effects greater than or comparable to GHGs in some regions. This finding is in opposition to previous results based on only aerosol reduction (Wang et al., 2016; Zhao et al., 2018).

In contrast to the three extreme precipitation indices described above, CDD represents the variability of extreme drought. In the Asian continent north of 30°N, the increase in total precipitation reduces CDD, particularly at high latitudes. However, CDD increases in NIN, the southeastern Tibetan Plateau, and the southern Yangtze River (Fig. 8a and b). Overall, CDD decreases by 0.5 days and 1.1 days under the SSP3-7.0 and SSP3-7.0-lowNTCF scenarios, respectively. Future reductions in non-methane SLCFs contribute to significant decreases in CDD in northwestern China, near the Hengduan Mountains, and the Indo-China Peninsula. CDD decreases by 1.4 days in (SWC) due to a significant increase in the frequency and intensity of heavy precipitation, and the sign of the results shows good agreement among models (Fig. 9e). Similarly, the changes in CDD due to non-methane SLCF reductions in some regions are comparable to the impacts of GHG forcing. Notably, the increases in CDD in India and eastern China are accompanied by increases in the frequency and intensity of extreme precipitation, which may be related to the probability distribution of future precipitation. A decrease in light rainfall and increase in heavy rainfall will lead to simultaneous increases in CDD and extreme precipitation (Wang et al., 2016). Zhu et al. (2021) showed that

https://doi.org/10.5194/acp-2022-422
Preprint. Discussion started: 5 July 2022


Atmospheric Chemistry and Physics Discussions

extreme precipitation in SC increases significantly while droughts become more severe under the SSP3-7.0 and SSP5-8.5 scenarios, suggesting that the future precipitation distribution in SC could be more heterogeneous under high SSP scenarios.

In general, along with the increase in average temperature, future reductions in the emissions of non-methane SLCFs will increase the intensity and frequency of extreme precipitation and decrease the occurrence of extreme droughts in Asia. Previous studies have shown that the increase in aerosol emissions since the 1950s may have contributed to the anomalous precipitation pattern of "southern flood/northern drought" reported in eastern China and reduced precipitation in India (Bollasina et al., 2011; Li et al., 2016; Zhao et al., 2018), which will likely be mitigated by future aerosol reductions. Based on the spatial patterns of extreme precipitation indices described above, future combined reductions of aerosols, ozone, and their precursors will lead to marked increases of R10, RX5day, and R95p along with a decrease in CDD in northern China, which is consistent with the spatial pattern of precipitation when only aerosol emissions reduction is considered. However, both extreme heavy precipitation and drought will increase in India. Consequently, our results indicate that future non-methane SLCF reductions may alleviate the observed precipitation anomaly pattern of "southern flood/northern drought" over eastern China, but may not have apparent mitigating effects on the precipitation reduction in India.

3.4 Population exposure to climate extremes in Asia

Extreme weather and climate events pose serious threats to human health, economic stability, and environmental sustainability, particularly in densely populated areas. Sustained warming of the climate will exacerbate climate extremes and the associated risks (Diffenbaugh et al., 2017; Sun et al., 2021). Based on the analysis presented above, reduction of non-methane SLCFs will further increase the frequency, intensity, and duration of extreme temperature and precipitation occurrences in Asia. Next, we analyze the changes in population exposure to extreme high temperature (TX90p) and heavy precipitation (R95p) under both future scenarios (Fig. 10).

Considering population growth and increased frequency of climate extremes, the total population exposed to TX90p and R95p show similar spatial patterns under the SSP3-7.0 and SSP3-7.0-lowNTCF scenarios, with the largest increases in India and eastern China (Fig. 10a, b, d, and e). Quantitatively, with the same population growth, a significantly greater population will be exposed to extreme temperature than to extreme heavy precipitation due to the higher frequency of extreme temperature events than extreme heavy precipitation events in the future. Under the SSP3-7.0 scenario, the largest increases in the population exposed to extreme temperature occur in India and eastern China, with a maximum increase greater than 6×10^8 person-days, while the increases in the population exposed to extreme precipitation exceed 4.5×10^7 person-days in India and are relatively small in eastern China ($>1.5 \times 10^7$ person-days). Compared to the SSP3-7.0 scenario, future non-methane SLCF reduction will increase the population exposed to extreme temperature by more than 3.5×10^8 person-days in NIN, followed by 1.5×10^8 person-days in NC and the SCB. In addition, future non-methane SLCF reductions will significantly increase the population exposed to extreme precipitation in India, the SCB, and the middle and lower reaches of the Yangtze River, reaching values greater than 6×10^6 person-days.

https://doi.org/10.5194/acp-2022-422
Preprint. Discussion started: 5 July 2022


Atmospheric Chemistry and Physics Discussions

Future changes in population exposure to climate extremes are affected by climate, population, and climate-population interactions according to equation (1) presented above. Under the SSP3 scenario, the population in India increases significantly by 2040 relative to 2000. This change is particularly sharp in NIN, which experiences an increase of more than 5 million people, followed by more than 1 million people in the SCB, NC and SC (data not shown). We attribute the changes in population exposure to three major factors (Figs. 11 and 12).

The increases in population exposed to extreme high temperatures are dominated by changes in climate factors under both the SSP3-7.0 and SSP3-7.0-lowNTCF scenarios in the four selected regions (Fig. 11). This result suggests that climate change is the primary driver of population exposure to extreme temperature events, followed by changes in the climate-population interaction factor, with population change contributing the least. Future non-methane SLCF reductions increase population exposure to TX90p by $(32.2 \pm 11.4) \times 10^7$ person-days in NIN, $(10.3 \pm 5.2) \times 10^7$ person-days in NC, $(7.5 \pm 6.9) \times 10^7$ person-days in the SCB, and $(6.3 \pm 4.7) \times 10^7$ person-days in SC, respectively.

The climate factor is also the largest contributor to the increase in population exposure, followed by the climate-population interaction factor and the population factor in NC, the SCB, and SC (Fig. 12b-d). By contrast, the population factor becomes dominant in NIN, indicating that population growth is the main cause of increased population exposure in that region, followed by changes in the climate factor and climate-population interaction factor (Fig. 12a). Notably, in the SCB, greater changes in population exposure are caused by non-methane SLCF reductions than by the continued increase in GHGs (Fig. 12c). Future non-methane SLCF reductions increase total population exposure to R95p by $(6.7 \pm 7.8) \times 10^6$ person-days in NIN, $(3.6 \pm 3.8) \times 10^6$ person-days in NC, $(4.9 \pm 4.8) \times 10^6$ person-days in the SCB, and $(3.4 \pm 3.7) \times 10^6$ person-days in SC.

4 Discussion and conclusions

This study quantitatively assesses the impacts of reductions in emissions of non-methane SLCFs (including aerosols, ozone, and their precursors) on Asian climate extremes and the associated population exposure risks during 2031–2050 using MME simulations under the SSP3-7.0 and SSP3-7.0-lowNTCF scenarios from AerChemMIP. Our results show that non-methane SLCF reductions will exacerbate the warming effect caused by GHGs, resulting in increases in extreme temperature and precipitation events. These results are consistent with previous studies that have considered only aerosol reductions (Wang et al., 2016; Samset et al., 2018; Luo et al., 2020). Future reductions in non-methane SLCFs during 2031–2050 are predicted to cause a global mean ERF of 0.23 W m^{-2} and an increase of 0.19 K in global average SAT relative to 1995–2014 based on the MME results.

The additional warming caused by the reduction of non-methane SLCF emissions increases domain-averaged TXx by 0.3 K, TX90p by 4.8%, TR by 1.7 days, and WSDI by 1.0 days across Asia. Regionally, TXx, TX90p, and WSDI show their largest increases in NIN and NC, reaching 0.5 K, 8.5%, and 2.8 days and 0.4 K, 5.9%, and 3.0 days, respectively. The increase in TX90p due to non-methane SLCF mitigation is comparable to that caused by GHG emissions in some regions. The models agree on the sign of the change in TR across regions, with the largest increases in NC and the SCB reaching 5.1 and 4.9 days,

https://doi.org/10.5194/acp-2022-422
Preprint. Discussion started: 5 July 2022


Atmospheric Chemistry and Physics Discussions

respectively. Overall, the warming trends driven by the combined reductions of aerosols, ozone, and their precursors are similar to the trends driven only by aerosol reductions. In addition, population exposure to TX90p associated with future non-methane SLCF reductions is greatest in NIN, at $(32.2 \pm 11.4) \times 10^7$ person-days.

For extreme precipitation, future non-methane SLCF reductions increase domain-averaged R10 by 1.3 days, RX5day by 0.8 mm, and R95p by 16.4 mm in Asia. In SWC, R10, RX5day, and R95p increase by 3.03 days, 2.2 mm, and 39.5 mm, and these increases are greater or comparable to the effects of GHGs. By contrast, CDD decreases by 1.4 days in SWC due to significant increases in the frequency and intensity of heavy precipitation events. Notably, large differences in extreme precipitation changes are found at the regional scale in response to reductions of non-methane SLCFs and only aerosols, with changes in opposite directions observed in some regions. This discrepancy may be attributed to ozone and aerosol interactions, which may be further assessed via model simulations with both coupled and uncoupled experiments in the future. The spatial pattern of changes in the total population exposed to R95p due to non-methane SLCF reductions is largely consistent with the distribution of TX90p, with the largest increases in India reaching $(6.7 \pm 7.8) \times 10^6$ person-days.

Notably, large biases may exist in SLCF emissions at the regional scale in global emissions scenarios due to insufficient consideration of local environmental policies (Tong et al., 2020). For example, the SSP-RCP global emissions scenarios used in CMIP6 do not fully consider the rapid pollution controls enacted in China since 2013 under the Air Pollution Prevention and Control Action Plan. Consequently, the emissions trends in the SSP scenarios after 2014 differ significantly from actual conditions in China (Wang et al., 2021; Tong et al., 2020), which may lead to underestimation of the impact of SLCF emissions reductions in China. In addition, reduction of GHGs emissions is not considered in the SSP3-7.0-lowNTCF scenario. GHGs share many common sources with SLCFs, such as the combustion of fossil fuels such as coal and oil. Therefore, emissions reductions aimed at achieving global carbon neutrality will inevitably result in further reductions in SLCF emissions, as demonstrated in the SSP1-1.9 and SSP1-2.6 scenarios (Gidden et al., 2019), which may lead to greater impacts of SLCFs on climate. This study highlights the effects of future reduction of non-methane SLCF emissions on climate change and associated exposure risks at the regional scale.

Data availability. The CMIP6 Historical and AerChemMIP model data can be freely downloaded from https://esgf-node.llnl.gov/projects/cmip6. Gridded population datasets for the base year and future under SSP3 scenario are publicly available at https://www.cgd. ucar.edu/iam/modeling/spatial-population-scenarios.

Author contributions. ZW conceived the study. YL performed the analysis. YL, ZW, and YL led the paper writing. All authors provided comments and contributed to the text.

Competing interests. The authors declare that they have no conflict of interest.

https://doi.org/10.5194/acp-2022-422
Preprint. Discussion started: 5 July 2022

Acknowledgments. This study was supported by the National Natural Science Foundation of China (41875179) and the Science and technology development fund of CAMS (2022KJ004).

References

Allen, J. R., Turnock, S., Nabat, P., Neubauer, D., Lohmann, U., Olivié, D., Oshima, N., Michou, M., Wu, T., Zhang, J., Takemura, T., Schulz, M., Tsigaridis, K., E. Bauer, S., Emmons, L., Horowitz, L., Naik, V., Van Noije, T., Bergman, T., Lamarque, J. F., Zanis, P., Tegen, I., M. Westervelt, D., Le Sager, P., Good, P., Shim, S., O'Connor, F., Akritidis, D., Georgoulias, A. K., Deushi, M., T. Sentman, L., G. John, J., Fujimori, S., and J. Collins, W.: Climate and air quality impacts due to mitigation of non-methane near-term climate forcers, Atmos. Chem. Phys., 20, 9641–9663, https://doi.org/10.5194/acp-20-9641-2020, 2020.

An, J., Fu, B., Li W., Peng, S., Li, B.: Future Prediction of Typical Extreme Climatic Indices and Population Exposure to High Temperature in East Asia. Acta Scientiarum Naturalium Universitatis Pekinensis, 56, 884–892, https://doi.org/10.13209/j.0479-8023.2020.071, 2020.

Apte, J. S., Marshall, J. D., Cohen, A. J., and Brauer, M.: Addressing Global Mortality from Ambient PM2.5., Environ. Sci. Technol., 49, 8057–8066, https://doi.org/10.1021/acs.est.5b01236, 2015.

Baker, L., Collins, W., Olivié, D., Cherian, R., Hodnebrog, Ø., Myhre, G., and Quaas, J.: Climate responses to anthropogenic emissions of short-lived climate pollutants, Atmos. Chem. Phys., 15, https://doi.org/10.5194/acp-15-8201-2015, 2015.

Bollasina, M. A., Yi, M., and V., R.: Anthropogenic Aerosols and the Weakening of the South Asian Summer Monsoon, Science, 334, 502–505, https://doi.org/10.1126/science.1204994, 2011.

Chang, W., Liao, H., and Wang, H.: Climate responses to direct radiative forcing of anthropogenic aerosols, tropospheric ozone, and long-lived greenhouse gases in eastern China over 1951–2000, Adv. Atmos. Sci., 26, 748–762, https://doi.org/10.1007/s00376-009-9032-4, 2009.

Chen, H. and Sun, J.: Increased population exposure to extreme droughts in China due to 0.5 °C of additional warming, Environ. Res. Lett., 14, https://doi.org/10.1088/1748-9326/ab072e, 2019.

Chen, H. and Sun, J.: Increased population exposure to precipitation extremes in China under global warming scenarios, Atmos. Ocean. Sci. Lett., 13, 63–70, https://doi.org/10.1080/16742834.2020.1697168, 2020.

Chen, H., Sun, J., and Li, H.: Increased population exposure to precipitation extremes under future warmer climates, Environ. Res. Lett., 15, https://doi.org/10.1088/1748-9326/ab751f, 2020.

Chen, J., Liu, Y., Pan, T., Liu, Y., Sun, F., and Ge, Q.: Population exposure to droughts in China under the 1.5°C global warming target, Earth Syst. Dyn., 9, 1097–1106, https://doi.org/10.5194/esd-9-1097-2018, 2018.

Chuwah, C., van Noije, T., van Vuuren, D. P., Le Sager, P., and Hazeleger, W.: Global and regional climate impacts of future aerosol mitigation in an RCP6.0-like scenario in EC-Earth, Clim. Change, 134, 1–14, https://doi.org/10.1007/s10584-015-1525-9, 2016.

Collins, J. W., Lamarque, J. F., Schulz, M., Boucher, O., Eyring, V., Hegglin, I. M., Maycock, A., Myhre, G., Prather, M., Shindell, D., and Smith, J. S.: AerChemMIP: Quantifying the effects of chemistry and aerosols in CMIP6, Geosci. Model Dev., 10, 585–607, https://doi.org/10.5194/gmd-10-585-2017, 2017.

Diffenbaugh N. S., Singh, D., Mankin. J. S., Horton, D.E., H. D., Swain, D.L., Touma, D,. Charland, A., Liu, Y., Haugen, M., Tsang, M., and Rajaratnam, B.: Quantifying the influence of global warming on unprecedented extreme climate events, Proc. Natl. Acad. Sci., 114, 4881–4886, https://doi.org/10.1073/pnas.1618082114, 2017.

Dong, B., Wilcox, L. J., Highwood, E. J., and Sutton, R. T.: Impacts of recent decadal changes in Asian aerosols on the East Asian summer monsoon: roles of aerosol–radiation and aerosol–cloud interactions, Clim. Dyn., 53, 3235–3256, https://doi.org/10.1007/s00382-019-04698-0, 2019.

Fischer, E. M. and Schär, C.: Consistent geographical patterns of changes in high-impact European heatwaves, Nat. Geosci., 3, 398–403, https://doi.org/10.1038/ngeo866, 2010.

Forster, P. M., Richardson, T., Maycock, A. C., Smith, C. J., Samset, B. H., Myhre, G., Andrews, T., Pincus, R., and Schulz, M.: Recommendations for diagnosing effective radiative forcing from climate models for CMIP6, J. Geophys. Res. Atmos., 121, 12,412-460,475, https://doi.org/https://doi.org/10.1002/2016JD025320, 2016.

Frich, P.L., Alexander, L., Della-Marta, P., Gleason, B., Haylock, M., Klein, T., and Peterson, T.C.: Observed coherent changes in climatic extremes during 2nd half of the 20th century, Clim. Res., 19, https://doi.org/10.3354/cr019193, 2002.

Gidden, M. J., Riahi, K., Smith, S. J., Fujimori, S., Luderer, G., Kriegler, E., van Vuuren, D. P., van den Berg, M., Feng, L., Klein, D., Calvin, K., Doelman, J. C., Frank, S., Fricko, O., Harmsen, M., Hasegawa, T., Havlik, P., Hilaire, J., Hoesly, R., Horing, J., Popp, A., Stehfest, E., and Takahashi, K.: Global emissions pathways under different socioeconomic scenarios for use in CMIP6: a dataset of harmonized emissions trajectories through the end of the century, Geosci. Model Dev., 12, 1443–1475, https://doi.org/10.5194/gmd-12-1443-2019, 2019.

Gosling, S. N., Lowe, J. A., McGregor, G. R., Pelling, M., and Malamud, B. D.: Associations between elevated atmospheric temperature and human mortality: a critical review of the literature, Clim. Change, 92, 299–341, https://doi.org/10.1007/s10584-008-9441-x, 2009.

Hienola, A., Partanen, A. I., Pietikäinen, J. P., O'Donnell, D., Korhonen, H., Matthews, H. D., and Laaksonen, A.: The impact of aerosol emissions on the 1.5 °C pathways, Environ. Res. Lett., 13, 44011, https://doi.org/10.1088/1748-9326/aab1b2, 2018.

Hoesly, R. M., Smith, S. J., Feng, L., Klimont, Z., Janssens-Maenhout, G., Pitkanen, T., Seibert, J. J., Vu, L., Andres, R. J., Bolt, R. M., Bond, T. C., Dawidowski, L., Kholod, N., Kurokawa, J.-I., Li, M., Liu, L., Lu, Z., Moura, M. C. P., O'Rourke, P. R., and Zhang, Q.: Historical (1750–2014) anthropogenic emissions of reactive gases and aerosols from the Community Emissions Data System (CEDS), Geosci. Model Dev., 11, 369–408, https://doi.org/10.5194/gmd-11-369-2018, 2018.

https://doi.org/10.5194/acp-2022-422
Preprint. Discussion started: 5 July 2022


Atmospheric Chemistry and Physics Discussions

J. Allen, R., Turnock, S., Nabat, P., Neubauer, D., Lohmann, U., Olivié, D., Oshima, N., Michou, M., Wu, T., Zhang, J., Takemura, T., Schulz, M., Tsigaridis, K., E. Bauer, S., Emmons, L., Horowitz, L., Naik, V., Van Noije, T., Bergman, T., Lamarque, J. F., Zanis, P., Tegen, I., M. Westervelt, D., Le Sager, P., Good, P., Shim, S., O'Connor, F., Akritidis, D., Georgoulias, A. K., Deushi, M., T. Sentman, L., G. John, J., Fujimori, S., and J. Collins, W.: Climate and air quality impacts due to mitigation of non-methane near-term climate forcers, Atmos. Chem. Phys., 20, 9641–9663, https://doi.org/10.5194/acp-20-9641-2020, 2020.

Jones, B., O'Neill, B. C., McDaniel, L., McGinnis, S., Mearns, L. O., and Tebaldi, C.: Future population exposure to US heat extremes, Nat. Clim. Chang., 5, 652–655, https://doi.org/10.1038/nclimate2631, 2015.

Li, S., Wang, T., Zanis, P., Melas, D., and Zhuang, B.: Impact of Tropospheric Ozone on Summer Climate in China, J. Meteorol. Res., 32, 279–287, https://doi.org/10.1007/s13351-018-7094-x, 2018.

Li, Z., Lau, W., Ramanathan, V., Wu, G., Ding, Y., Manoj, M. G., Liu, J., Qian, Y., Li, J., Zhou, T., Fan, J., Rosenfeld, D., Ming, Y., Wang, Y., Huang, J., Wang, B., Xu, X., Lee, S.-S., Cribb, M., and Zhao, C.: Aerosol and Monsoon Climate Interactions over Asia: Aerosol and Monsoon Climate Interactions, Rev. Geophys., 54, https://doi.org/10.1002/2015RG000500, 2016.

Liao, H., Chang, W., and Yang, Y.: Climatic effects of air pollutants over china: A review, Adv. Atmos. Sci., 32, 115–139, https://doi.org/10.1007/s00376-014-0013-x, 2015.

Lin, L., Wang, Z., Xu, Y., and Fu, Q.: Sensitivity of precipitation extremes to radiative forcing of greenhouse gases and aerosols, Geophys. Res. Lett., 43, 9860–9868, https://doi.org/10.1002/2016GL070869, 2016.

Lin, L., Xu, Y., Wang, Z., Diao, C., Dong, W., and Xie, S.-P.: Changes in Extreme Rainfall Over India and China Attributed to Regional Aerosol-Cloud Interaction During the Late 20th Century Rapid Industrialization, Geophys. Res. Lett., 45, 7857–7865, https://doi.org/https://doi.org/10.1029/2018GL078308, 2018.

Luo, F., Wilcox, L., Dong, B., Su, Q., Chen, W., Dunstone, N., Li, S., and Gao, Y.: Projected near-term changes of temperature extremes in Europe and China under different aerosol emissions, Environ. Res. Lett., 15, 34013, https://doi.org/10.1088/1748-9326/ab6b34, 2020.

Malley, C. S., Henze, D. K., Kuylenstierna, J. C. I., Vallack, H. W., Davila, Y., Anenberg, S. C., Turner, M. C., and Ashmore, M. R.: Updated Global Estimates of Respiratory Mortality in Adults ≥30Years of Age Attributable to Long-Term Ozone Exposure., Environ. Health Perspect., 125, 87021, https://doi.org/10.1289/EHP1390, 2017.

Mu, J. and Wang, Z.: Responses of the East Asian summer monsoon to aerosol forcing in CMIP5 models: The role of upper-tropospheric temperature change, Int. J. Climatol., 41, 1555–1570, https://doi.org/10.1002/joc.6887, 2021.

Myhre, G., Shindell, D., Bréon, F.-M., Collins, W., Fuglestvedt, J., Huang, J., Koch, D., Lamarque, J.-F., Lee, D., Mendoza, B., Nakajima, T., Robock, A., Stephens, G., Takemura, T., and Zhang, H.: Anthropogenic and Natural Radiative Forcing, in Climate Change 2013: The Physical Science Basis. Contribution of Working Group I to the Fifth Assessment Report of the Intergovernmental Panel on Climate Change, Stocker, T. F., Qin, D., Plattner, G.-K., Tignor, M., Allen, S. K., Boschung, J.,

485 Nauels, A., Xia, Y., Bex, V., and Midgley, P. M. (Eds.), Tech. rep., Cam- bridge University Press, Cambridge, United Kingdom and New York, NY, USA, 2013.

Naik, V., Szopa, S., Adhikary, B., Artaxo, P., Berntsen, T., Collins, W. D., Fuzzi, S., Gallardo, L., Kiendler Scharr, A., Klimont, Z., Liao, H., Unger, N., and Zanis, P.: Short-Lived Climate Forcers. In: Climate Change 2021: The Physical Science Basis. Contribution of Working Group I to the Sixth Assessment Report of the Intergovernmental Panel on Climate Change, Masson-
490 Delmotte, V., Zhai, P., Pirani, A., Connors, S. L., Péan, C., Berger, S., Caud, N., Chen, Y., Goldfarb, L., Gomis, M. I., Huang, M., Leitzell, K., Lonnoy, E., Matthews, J. B. R., Maycock, T. K., Waterfield, T., Yelekçi, O., Yu R. and Zhou B. (Eds.), Cambridge University Press. In Press. 2021.

Pincus, R., Forster, P., and Stevens, B.: The Radiative Forcing Model Intercomparison Project (RFMIP): Experimental Protocol for CMIP6, Geosci. Model Dev. Discuss., 1–18, https://doi.org/10.5194/gmd-2016-88, 2016.

495 Pu, X., Wang, T. J., Huang, X., Melas, D., Zanis, P., Papanastasiou, D. K., and Poupkou, A.: Enhanced surface ozone during the heat wave of 2013 in Yangtze River Delta region, China, Sci. Total Environ., 603–604, 807–816, https://doi.org/https://doi.org/10.1016/j.scitotenv.2017.03.056, 2017.

Ramanathan, V., Li, F., Ramana, M. V, Praveen, P. S., Kim, D., Corrigan, C. E., Nguyen, H., Stone, E. A., Schauer, J. J., Carmichael, G. R., Adhikary, B., and Yoon, S. C.: Atmospheric brown clouds: Hemispherical and regional variations in long-
500 range transport, absorption, and radiative forcing, J. Geophys. Res. Atmos., 112, https://doi.org/https://doi.org/10.1029/2006JD008124, 2007.

Samset, B. H., Sand, M., Smith, C. J., Bauer, S. E., Forster, P. M., Fuglestvedt, J. S., Osprey, S., and Schleussner, C. F.: Climate Impacts From a Removal of Anthropogenic Aerosol Emissions, Geophys. Res. Lett., 45, 1020–1029, https://doi.org/10.1002/2017GL076079, 2018.

505 Sillmann, J., Kharin, V. V, Zwiers, F. W., Zhang, X., and Bronaugh, D.: Climate extremes indices in the CMIP5 multimodel ensemble: Part 2. Future climate projections, J. Geophys. Res. Atmos., 118, 2473–2493, https://doi.org/https://doi.org/10.1002/jgrd.50188, 2013.

Sun, S., Dai, T. L., Wang, Z. Y., Chou, J. M., Chao, Q. C., and Shi, P. J.: Projected increases in population exposure of daily climate extremes in eastern China by 2050, Adv. Clim. Chang. Res., https://doi.org/10.1016/j.accre.2021.09.014, 2021.

510 Sun, X., Ge, F., Fan, Y., Zhu, S., and Chen, Q.: Will population exposure to heat extremes intensify over Southeast Asia in a warmer world?, Environ. Res. Lett., 17, 44006, https://doi.org/10.1088/1748-9326/ac48b6, 2022.

Tong, D., Cheng, J., Liu, Y., Yu, S., Yan, L., Hong, C., Qin, Y., Zhao, H., Zheng, Y., Geng, G., Li, M., Liu, F., Zhang, Y., Zheng, B., Clarke, L., and Zhang, Q.: Dynamic projection of anthropogenic emissions in China: methodology and 2015--2050 emission pathways under a range of socio-economic, climate policy, and pollution control scenarios, Atmos. Chem. Phys., 20,
515 5729–5757, https://doi.org/10.5194/acp-20-5729-2020, 2020.

Wang, Z., Mu, J., Yang, M., and Yu, X.: Reexamining the mechanisms of East Asian summer monsoon changes in response to non-East Asian anthropogenic aerosol forcing, J. Clim., 33, 2929–2944, https://doi.org/10.1175/JCLI-D-19-0550.1, 2020.

Wang, Z., Lin, L., Xu, Y., Che, H., Zhang, X., Zhang, H., Dong, W., Wang, C., Gui, K., and Xie, B.: Incorrect Asian aerosols affecting the attribution and projection of regional climate change in CMIP6 models, npj Clim. Atmos. Sci., 4, 2, https://doi.org/10.1038/s41612-020-00159-2, 2021.

Wang, Z., Lin, L., Yang, M., and Guo, Z.: The Role of Anthropogenic Aerosol Forcing in Interdecadal Variations of Summertime Upper-Tropospheric Temperature Over East Asia, Earth's Futur., 7, 136–150, https://doi.org/10.1029/2018EF001052, 2019.

Wang, Z., Lin, L., Yang, M., and Xu, Y.: The effect of future reduction in aerosol emissions on climate extremes in China, Clim. Dyn., 47, 2885–2899, https://doi.org/10.1007/s00382-016-3003-0, 2016.

Wei, Y., Chen, X., Chen, H., Li, J., Wang, Z., Yang, W., Ge, B., Du, H., Hao, J., Wang, W., Li, J., Sun, Y., and Huang, H.: IAP-AACM v1.0: a global to regional evaluation of the atmospheric chemistry model in CAS-ESM, Atmos. Chem. Phys., 19, 8269–8296, https://doi.org/10.5194/acp-19-8269-2019, 2019.

Westervelt, D. M., Conley, A. J., Fiore, A. M., Lamarque, J. F., Shindell, D. T., Previdi, M., Mascioli, N. R., Faluvegi, G., Correa, G., and Horowitz, L. W.: Connecting regional aerosol emissions reductions to local and remote precipitation responses, Atmos. Chem. Phys., 18, 12461–12475, https://doi.org/10.5194/acp-18-12461-2018, 2018.

Westervelt, D. M., Horowitz, L. W., Naik, V., Golaz, J. C., and Mauzerall, D. L.: Radiative forcing and climate response to projected 21st century aerosol decreases, Atmos. Chem. Phys., 15, 12681–12703, https://doi.org/10.5194/acp-15-12681-2015, 2015.

Wilcox, L., Liu, Z., Samset, B., Hawkins, E., Lund, M., Nordling, K., Undorf, S., Bollasina, M., Ekman, A., Krishnan, S., Merikanto, J., and Turner, A.: Accelerated increases in global and Asian summer monsoon precipitation from future aerosol reductions, Atmos. Chem. Phys., 1–30, https://doi.org/10.5194/acp-2019-1188, 2020.

Xie, B., Zhang, H., Wang, Z., Zhao, S., and Fu, Q.: A modeling study of effective radiative forcing and climate response due to tropospheric ozone, Adv. Atmos. Sci., 33, 819–828, https://doi.org/10.1007/s00376-016-5193-0, 2016a.

Xie, X., Wang, H., Liu, X., Li, J., Wang, Z., and Liu, Y.: Distinct effects of anthropogenic aerosols on the East Asian summer monsoon between multidecadal strong and weak monsoon stages, J. Geophys. Res. Atmos., 121, 7026–7040, https://doi.org/https://doi.org/10.1002/2015JD024228, 2016b.

Yang, D., Zhao, S., Zhang, H., and Shen, X.Y.: Simulation of global distribution of temporal and spatial variation of PM2.5 concentration in the future, Zhongguo Huanjing Kexue/China Environ. Sci., 37, 1201–1212, 2017.

Zanis, P., Akritidis, D., Georgoulias, K. A., Allen, J. R., Bauer, E. S., Boucher, O., Cole, J., Johnson, B., Deushi, M., Michou, M., Mulcahy, J., Nabat, P., Olivié, D., Oshima, N., Sima, A., Schulz, M., Takemura, T., and Tsigaridis, K.: Fast responses on pre-industrial climate from present-day aerosols in a CMIP6 multi-model study, Atmos. Chem. Phys., 20, 8381–8404, https://doi.org/10.5194/acp-20-8381-2020, 2020.

Zhang, H., Xie, B., and Wang, Z.: Effective Radiative Forcing and Climate Response to Short-Lived Climate Pollutants Under Different Scenarios, Earth's Futur., 6, 857–866, https://doi.org/10.1029/2018EF000832, 2018.

https://doi.org/10.5194/acp-2022-422
Preprint. Discussion started: 5 July 2022

Atmospheric Chemistry and Physics Discussions

Zhao, A. D., Stevenson, D. S., and Bollasina, M. A.: The role of anthropogenic aerosols in future precipitation extremes over the Asian Monsoon Region, Clim. Dyn., 52, 6257–6278, https://doi.org/10.1007/s00382-018-4514-7, 2018.

Zhao, J., Su, B., Mondal, S. K., Wang, Y., Tao, H., and Jiang, T.: Population exposure to precipitation extremes in the Indus River Basin at 1.5 °C, 2.0 °C and 3.0 °C warming levels, Adv. Clim. Chang. Res., 12, 199–209, https://doi.org/10.1016/j.accre.2021.03.005, 2021.

Zhou, B., and Qian, J.: Changes of weather and climate extremes in the IPCC AR6, Adv. Clim. Chang. Res., 17, 713–718, https://doi.org/10.12006/j.issn.1673-1719.2021.167, 2021

Zhu, X., Lee, S. Y., Wen, X., Ji, Z., Lin, L., Wei, Z., Zheng, Z., Xu, D., and Dong, W.: Extreme climate changes over three major river basins in China as seen in CMIP5 and CMIP6, Clim. Dyn., 57, 1187–1205, https://doi.org/10.1007/s00382-021-05767-z, 2021.

https://doi.org/10.5194/acp-2022-422
Preprint. Discussion started: 5 July 2022

Atmospheric Chemistry and Physics Discussions

Model	Institution	Country	Atmospheric resolution (Longitude ×Latitude)	realizations
BCC-ESM1	Beijing Climate Centre (BCC)	China	2.81°×2.81°	3
CESM2-WACCM	National Center for Atmospheric Research (NCAR)	America	1.25°×0.94°	3
GISS-E2-1-G	Goddard Institute for Space Studies (GISS)	America	2.0°×2.5°	3
GFDL-ESM4	Geophysical Fluid Dynamics Laboratory (GFDL)	America	1.25°×1.0°	1
EC-Earth3-AerChem	European consortium of meteorological services, research institutes and high-performance computing centers (EC-Earth consortium)	European consortium	0.70°×0.70°	2
MRI-ESM2-0	Meteorological Research Institute (MRI)	Japan	1.87°×1.87°	3
UKESM1-0-LL	Met Office Hadley Centre (MOHC)	England	1.88°×1.88°	3

Table 1: Summary of CMIP6 models used in this study.

https://doi.org/10.5194/acp-2022-422
Preprint. Discussion started: 5 July 2022


Atmospheric Chemistry and Physics Discussions

Index Name	Index Definition	Units
The hottest day (TXx)	Annual average of the monthly maximum value of daily maximum temperature	K
The coldest day (TNn)	Annual average of monthly minimum value of daily maximum temperature	K
Warm days (TX90p)	Percentage of days with daily maximum temperature > 90% percentile	%
Warm nights (TN90p)	Percentage of days with daily minimum temperature > 90% percentile	%
Tropical nights (TR)	Annual count of days when daily minimum temperature > 20°C.	days
Warm spell duration (WSDI)	Annual count of days with at least 6 consecutive days when daily maximum temperature > 90th percentile	days
Maximum consecutive 5-day precipitation (RX5day)	Monthly maximum consecutive 5-day precipitation	mm
Total wet-day precipitation (R95p)	Annual total precipitation on days when daily precipitation >95th percentile.	mm
Heavy precipitation days (R10)	Annual count of days when precipitation ≥ 10mm	days
Consecutive dry days (CDD)	The maximum length of dry spell, the maximum number of consecutive days with precipitation < 1mm	days

Table 2: Definitions of the extreme climate indices used in this study.

https://doi.org/10.5194/acp-2022-422
Preprint. Discussion started: 5 July 2022

Atmospheric Chemistry and Physics Discussions

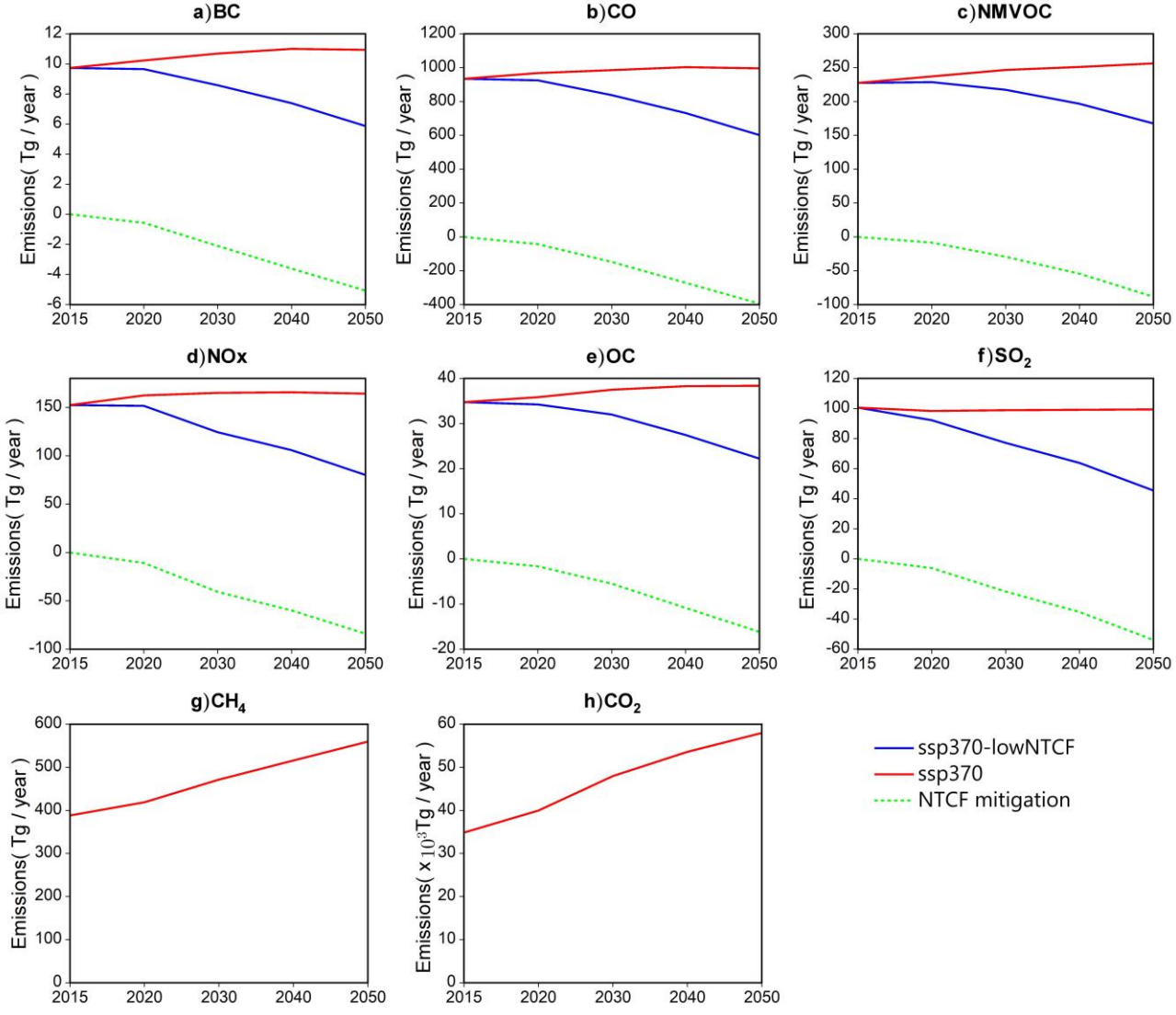

565 **Figure 1: Time series of global annual emissions of (a) BC, (b) CO, (c) NMVOC, (d) NOx, (e) OC, (f) SO_2, (g) CH_4, and (h) CO_2 from 2015-2050 under the SSP3-7.0 (red solid line) and SSP3-7.0-lowNTCF (blue solid line) scenarios. The green dashed lines represent the emission differences between the two scenarios.**

https://doi.org/10.5194/acp-2022-422
Preprint. Discussion started: 5 July 2022

Atmospheric Chemistry and Physics Discussions

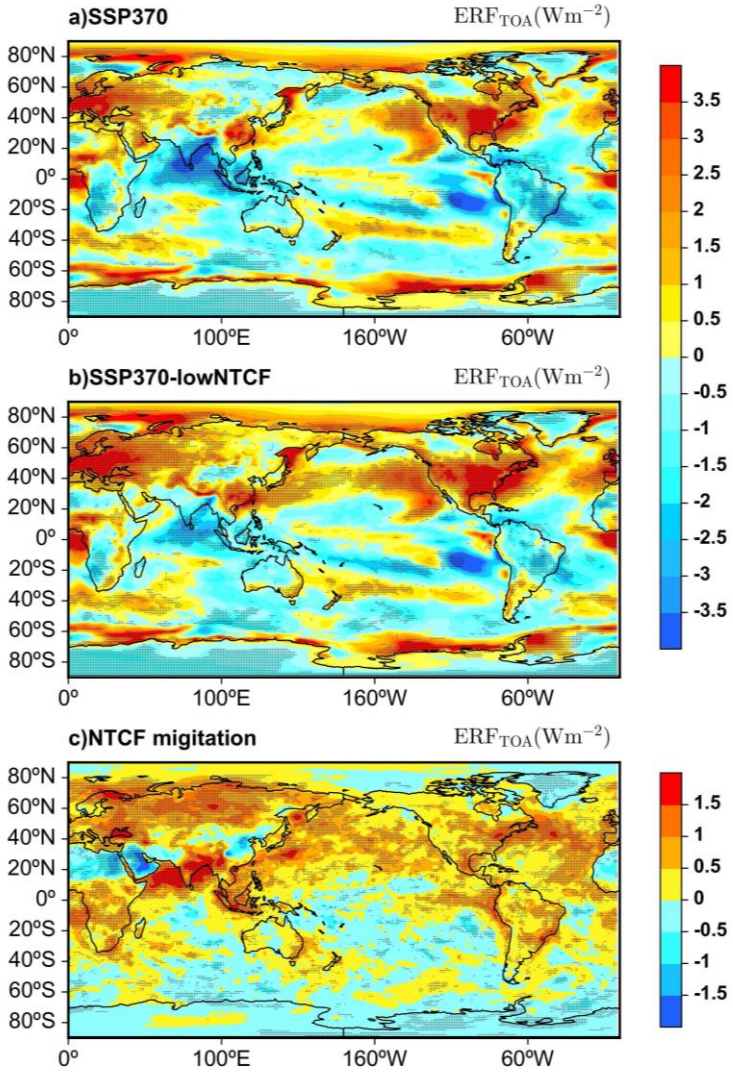

Figure 2: Spatial patterns of ERFs during 2031-2050 under the (a) SSP3-7.0 and (b)SSP3-7.0-lowNTCF scenarios and (c) only caused by the non-methane SLCFs reductions relative to 1995-2014 (units: W m^{-2}). The dotted regions indicate that more than 60% of the models agree on the sign.

https://doi.org/10.5194/acp-2022-422
Preprint. Discussion started: 5 July 2022

Atmospheric Chemistry and Physics Discussions

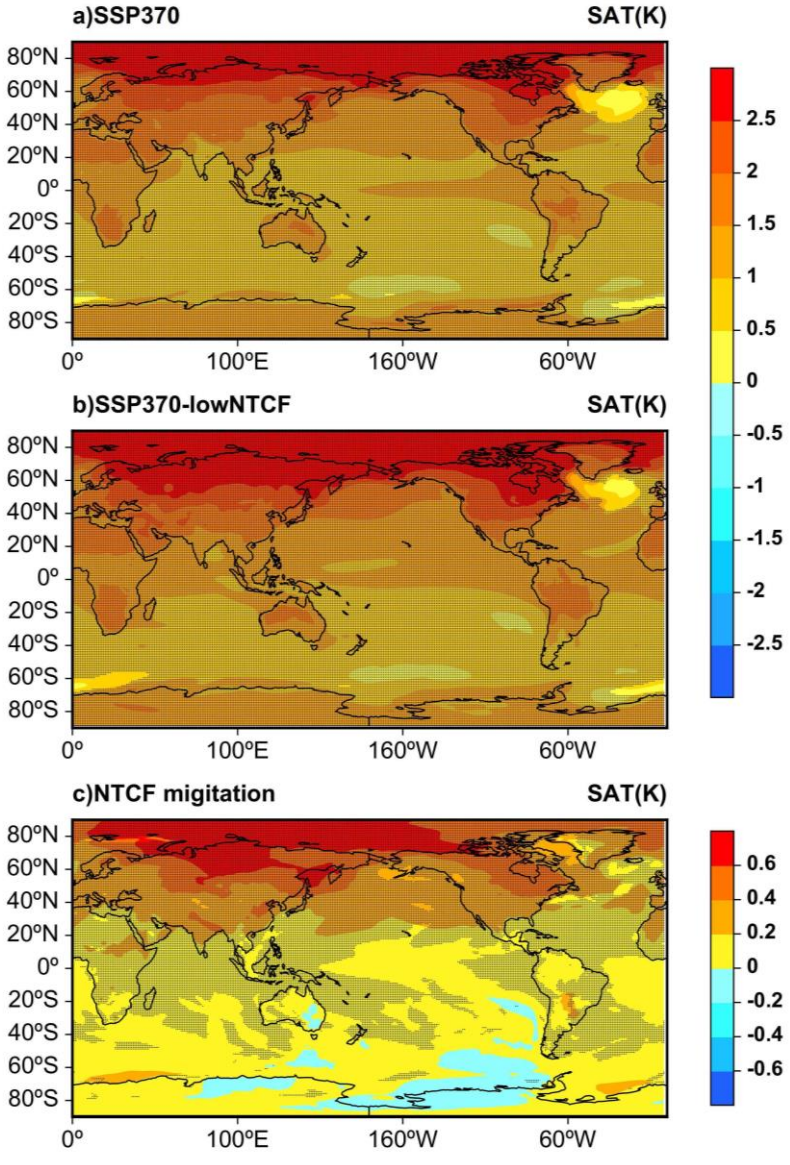

Figure 3: Spatial patterns of changes in SATs during 2031-2050 under the (a) SSP3-7.0 and (b) SSP3-7.0-lowNTCF scenarios and (c) only caused by the non-methane SLCFs reductions relative to 1995-2014surface air (units: K). The dotted regions indicate that more than 60% of the models agree on the sign.

https://doi.org/10.5194/acp-2022-422
Preprint. Discussion started: 5 July 2022

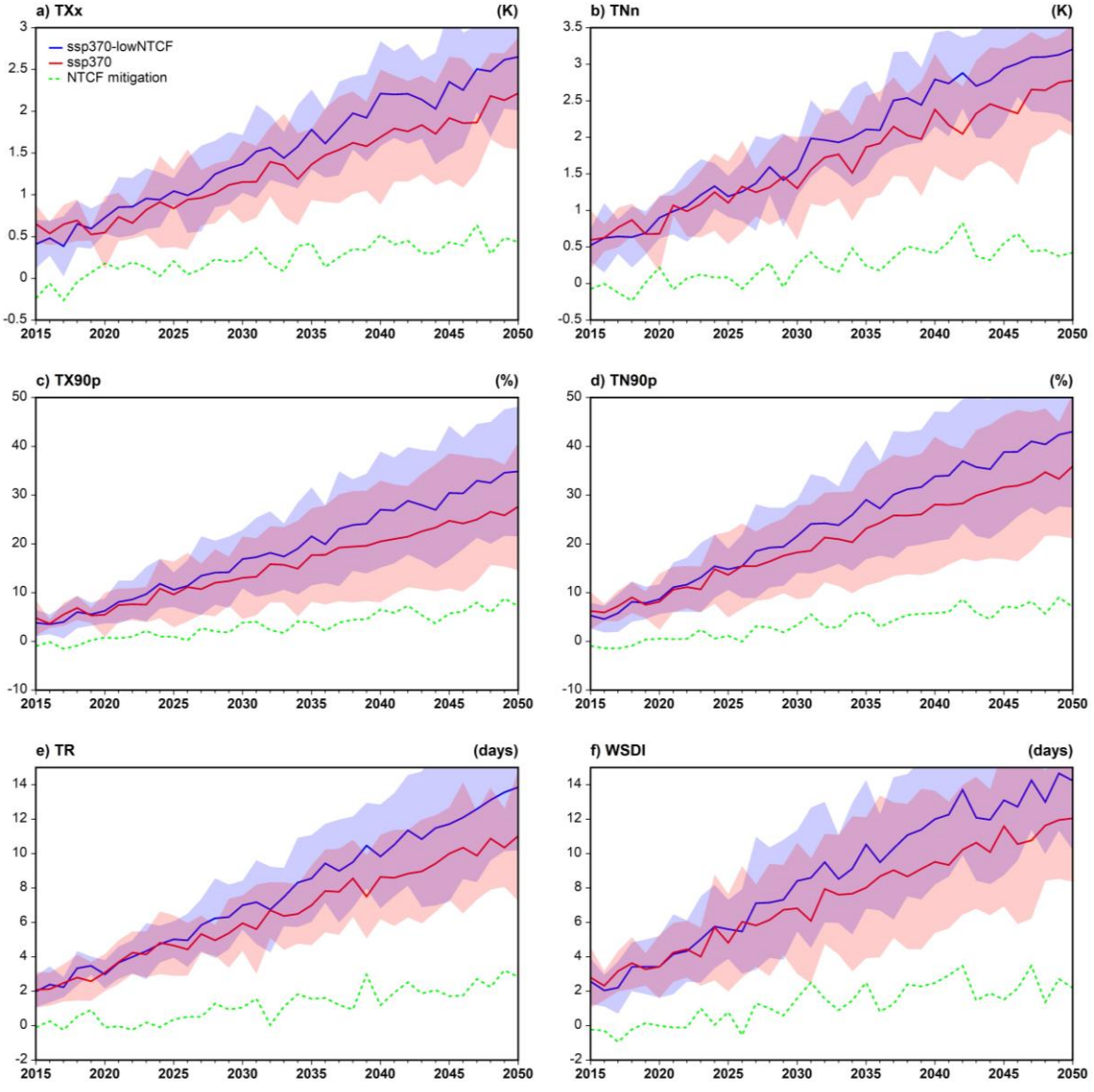

Figure 4: Time series of changes in annual mean extreme temperature indices averaged over Asia under the SSP3-7.0 (red) and SSP3-7.0-lowNTCF (blue) scenarios from 2015 to 2050 relative to 1995-2014. The green dashed lines represent the changes caused by the non-methane SLCFs reductions. The red and blue shading represents two standard deviations across models.

https://doi.org/10.5194/acp-2022-422
Preprint. Discussion started: 5 July 2022

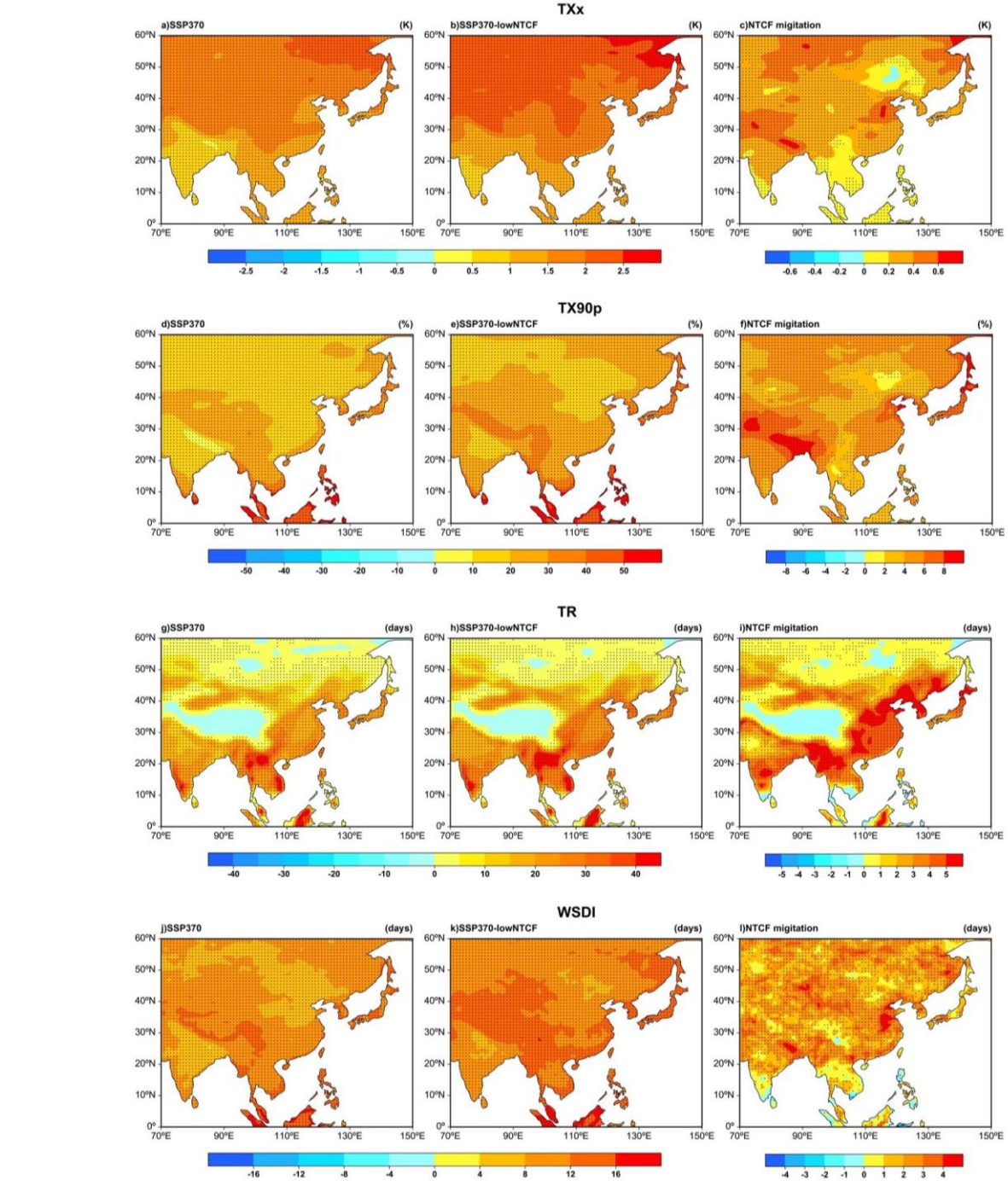

Figure 5: Spatial patterns of changes in TXx, TX90p, TR, and WSDI during 2031-2050 in Asia under the SSP3-7.0 (left column) and SSP3-7.0-lowNTCF (middle column) scenarios relative to 1995-2014. The right column represents changes caused by the non-methane SLCFs mitigation. The dotted regions indicate that more than 60% of the models agree on the sign.

https://doi.org/10.5194/acp-2022-422
Preprint. Discussion started: 5 July 2022

Atmospheric Chemistry and Physics Discussions

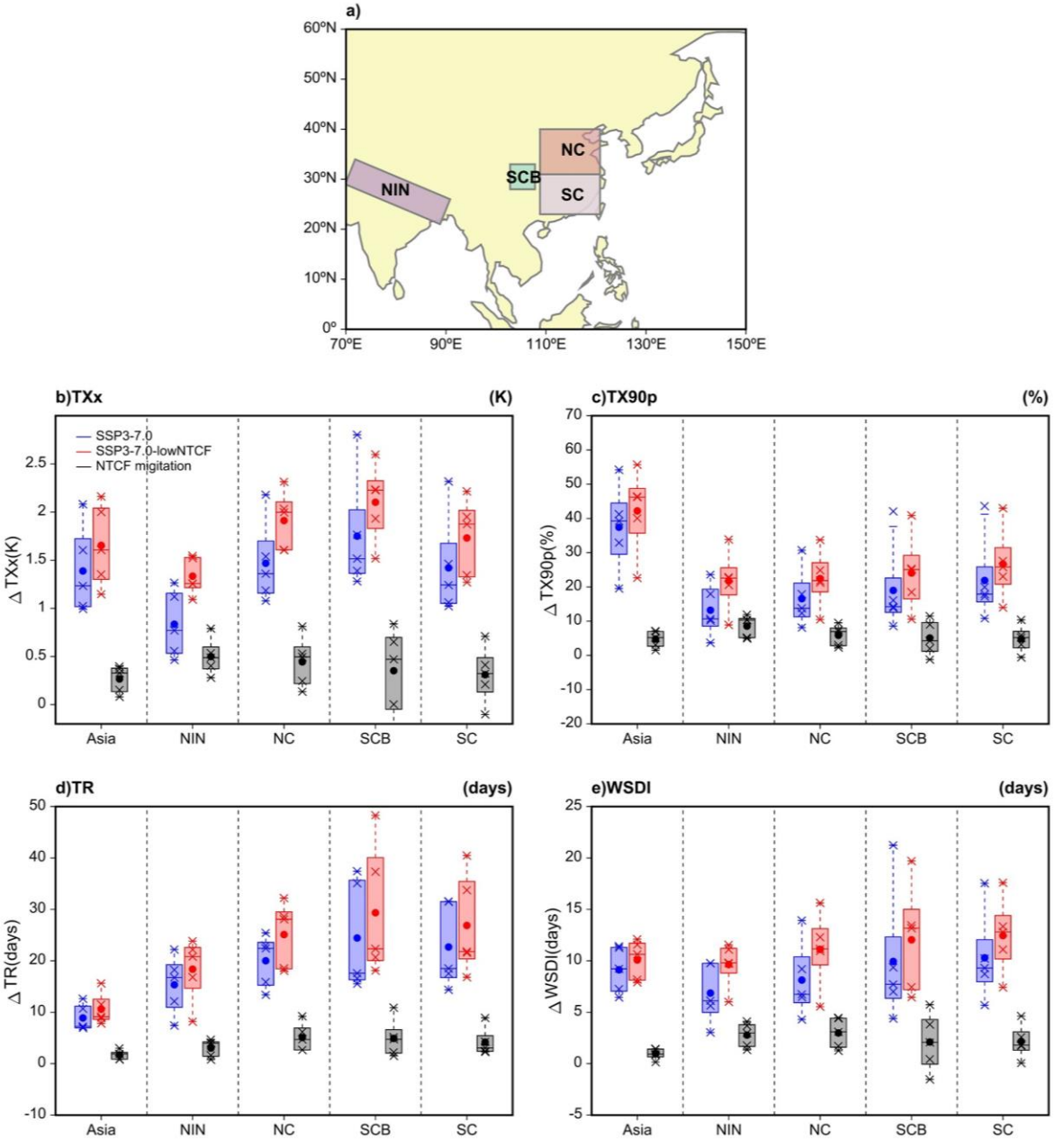

585 **Figure 6: Changes in TXx, TX90p, TR, and WSDI averaged over NIN, NC, SC, and SCB during 2031-2050 relative to 1995-2014 under the SSP3-7.0 (red) and SSP3-7.0-lowNTCF (blue) scenarios. The gray bars represent the changes caused by the non-methane SLCFs reductions. The star symbols indicate the individual models, and the boxes indicate the spread from the 25th to the 75th percentile of the models, with the center lines representing the median and the dot representing the mean values.**

https://doi.org/10.5194/acp-2022-422
Preprint. Discussion started: 5 July 2022

Atmospheric Chemistry and Physics Discussions

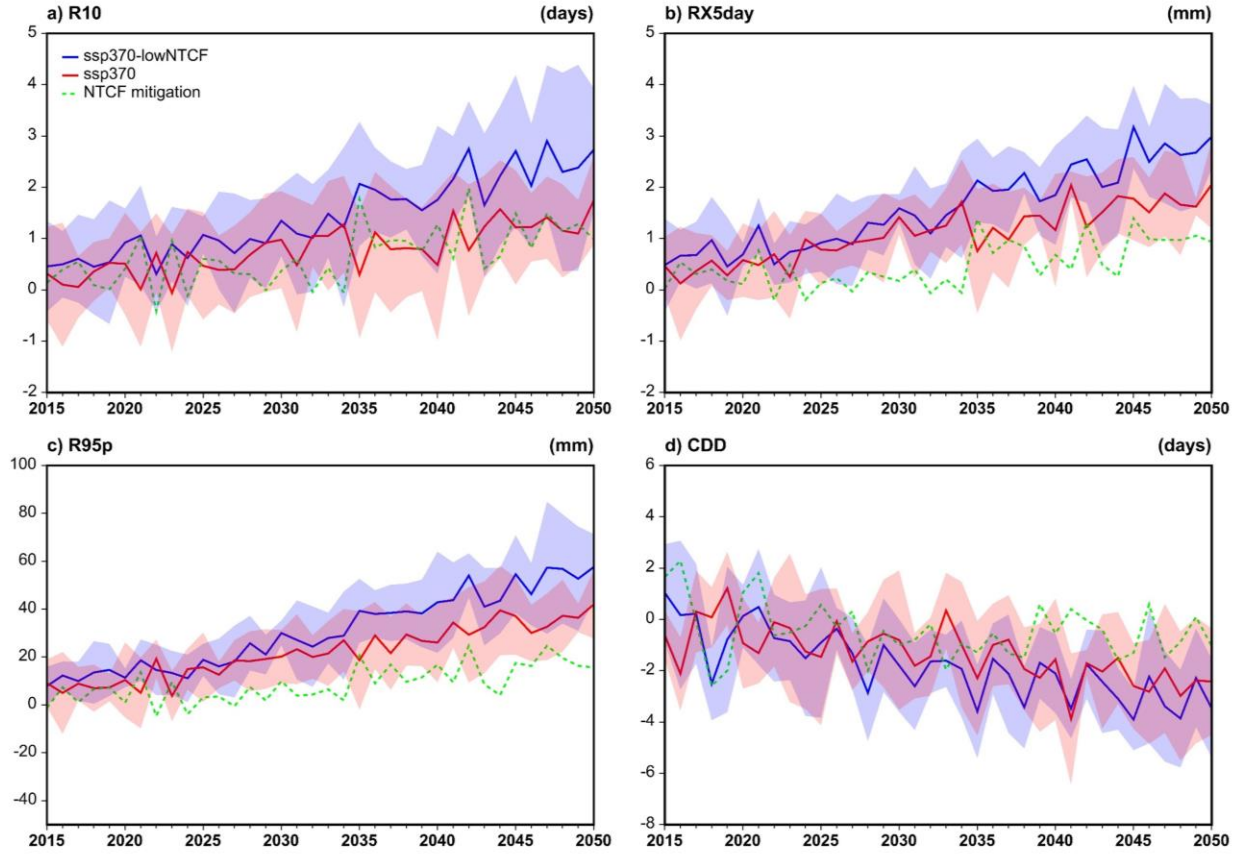

590 **Figure 7: Time series of changes in annual mean extreme precipitation indices averaged over Asia under the SSP3-7.0 (red) and SSP3-7.0-lowNTCF (blue) scenarios from 2015 to 2050 relative to 1995-2014. The green dashed lines represent the changes caused by the non-methane SLCFs reductions. The red and blue shading represents two standard deviations across models.**

https://doi.org/10.5194/acp-2022-422
Preprint. Discussion started: 5 July 2022

Atmospheric Chemistry and Physics Discussions

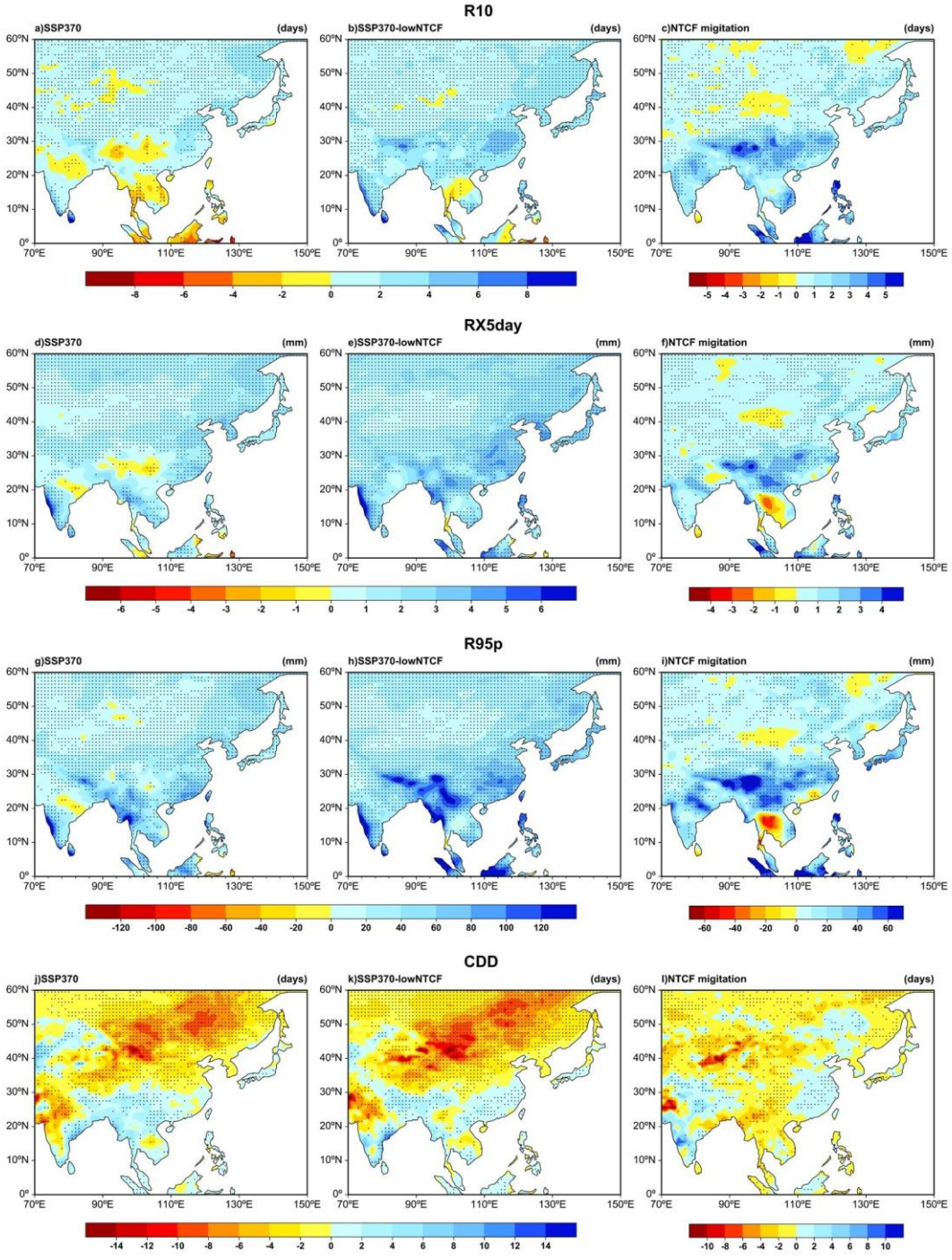

595 **Figure 8: Spatial patterns of changes in R10, RX5day, R95p, and CDD during 2031-2050 in Asia under the SSP3-7.0 (left column) and SSP3-7.0-lowNTCF (middle column) scenarios relative to 1995-2014. The right column represents changes caused by the non-methane SLCFs mitigation. The dotted regions indicate that more than 60% of the models agree on the sign.**

https://doi.org/10.5194/acp-2022-422
Preprint. Discussion started: 5 July 2022

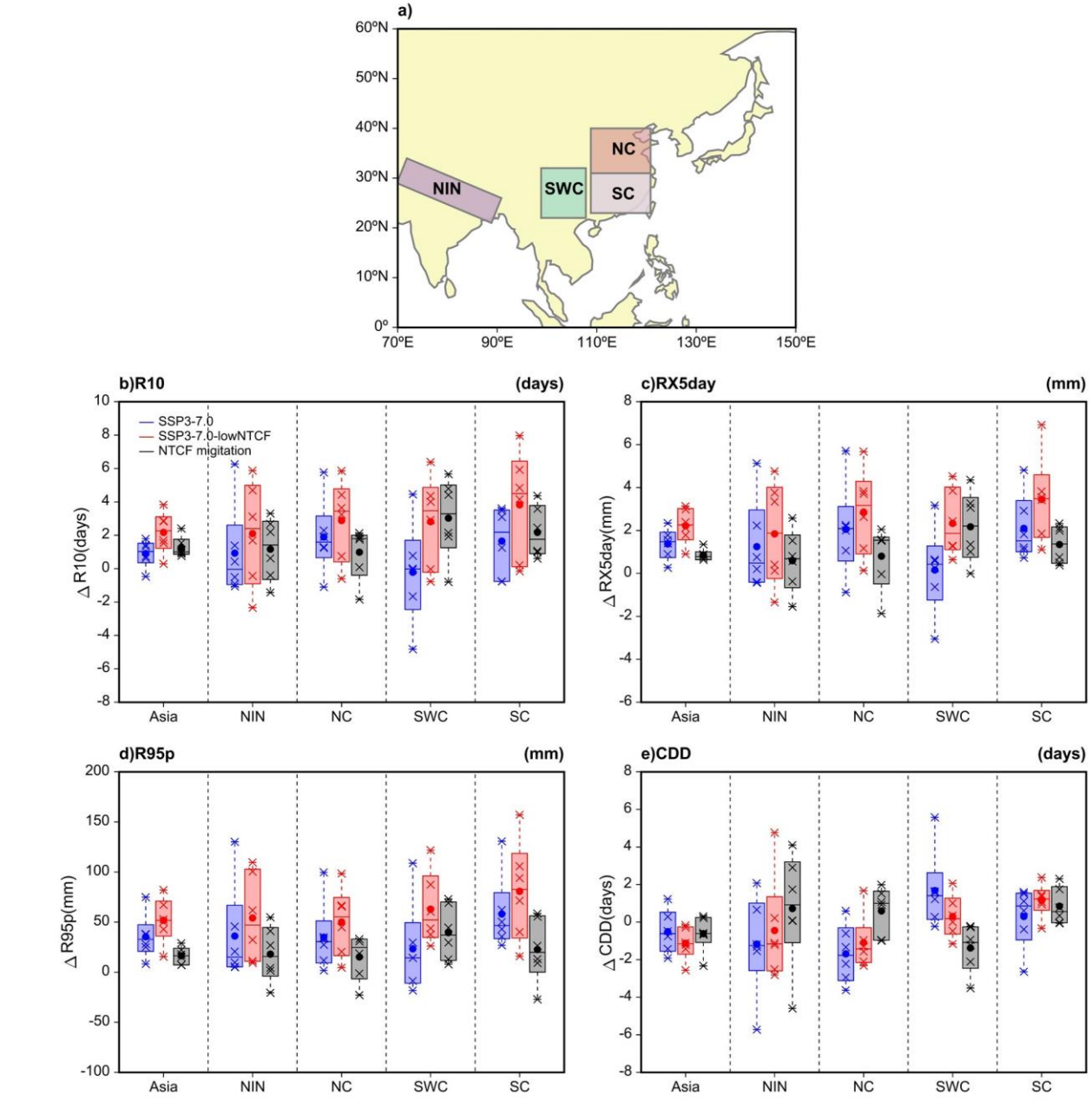

Figure 9: Changes in R10, RX5day, R95p, and CDD averaged over NIN, NC, SC, and SCB during 2031-2050 relative to 1995-2014 under the SSP3-7.0 (red) and SSP3-7.0-lowNTCF (blue) scenarios. The gray bars represent the changes caused by the non-methane SLCFs reductions. The star symbols indicate the individual models, and the boxes indicate the spread from the 25th to the 75th percentile of the models, with the center lines representing the median and the dot representing the mean values.

https://doi.org/10.5194/acp-2022-422
Preprint. Discussion started: 5 July 2022

Atmospheric Chemistry and Physics Discussions

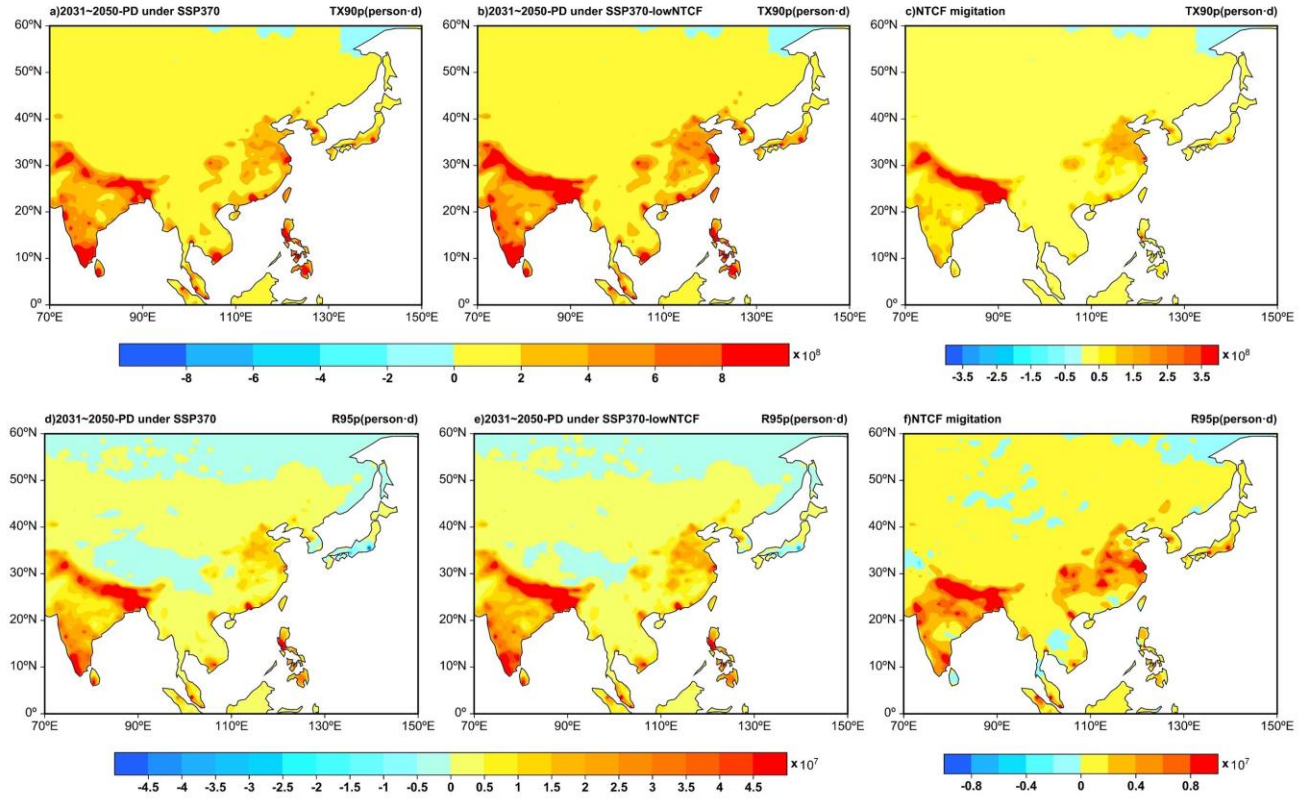

Figure 10: Spatial patterns of changes in population exposed to TX90p and R95p in Asia during 2031-2050 under the SSP3-7.0 (left) and SSP3-7.0-lowNTCF (middle) relative to 1995-2014 (units: person-days). The right column represents the changes caused by the non-methane SLCFs reductions.

https://doi.org/10.5194/acp-2022-422
Preprint. Discussion started: 5 July 2022

Atmospheric Chemistry and Physics Discussions

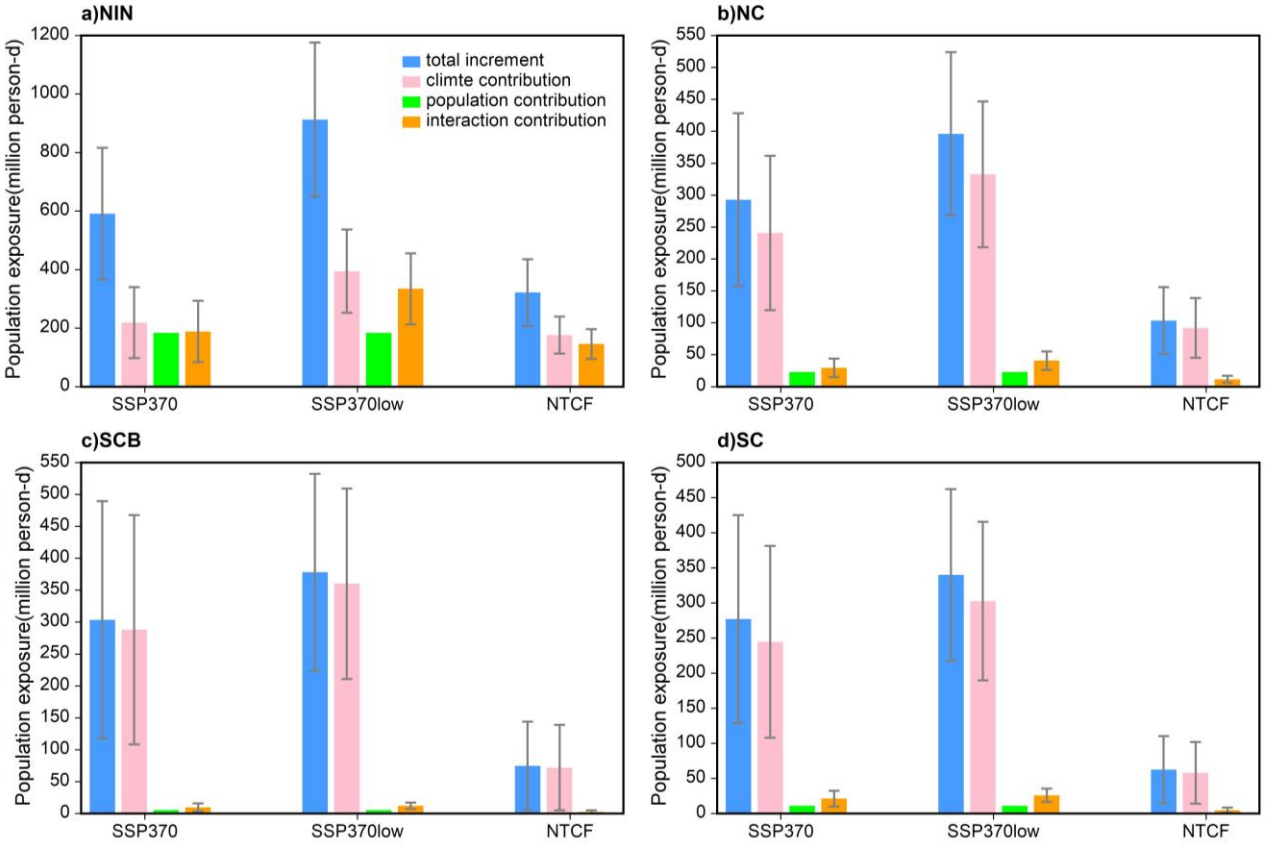

Figure 11: The total changes of population exposure to TX90p averaged over different regions under the SSP3-7.0 and SSP3-7.0-lowNTCF scenarios and its changes driven by the non-methane SLCFs reductions. The blue, yellow, and red bars represent the changes driven by climate change, population change, and population-climate interaction, respectively. The error bars denote two standard deviations across models.

https://doi.org/10.5194/acp-2022-422
Preprint. Discussion started: 5 July 2022

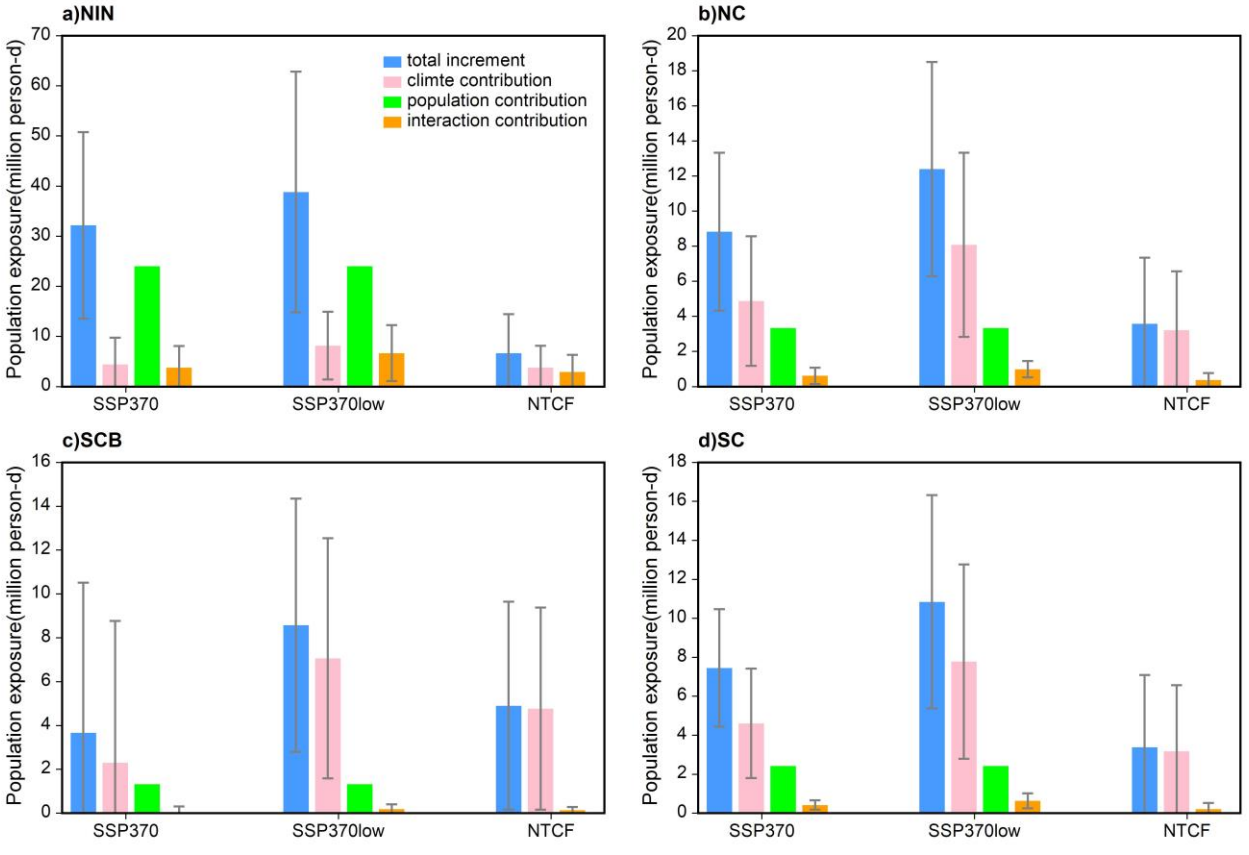

Figure 12: The total changes of population exposure to TX90p averaged over different regions under the SSP3-7.0 and SSP3-7.0-lowNTCF scenarios and its changes driven by the non-methane SLCFs reductions. The blue, yellow, and red bars represent the changes driven by climate change, population change, and population-climate interaction, respectively. The error bars denote two standard deviations across models.